

# The characteristics of flare- and CME-productive solar active regions

Ioannis Kontogiannis<sup>1</sup>

<sup>1</sup>Leibniz-Institut für Astrophysik Potsdam (AIP), An der Sternwarte 16 14482  
Potsdam, Germany

October 12, 2022

## Abstract

Solar flares and coronal mass ejections (CMEs) cause immediate and adverse effects on the interplanetary space and geospace. In an era of space-based technical civilization, the deeper understanding of the mechanisms that produce them and the construction of efficient prediction schemes are of paramount importance. The source regions of flares and CMEs exhibit some common morphological characteristics, such as  $\delta$ -spots, filaments and sigmoids, which are associated with strongly sheared magnetic polarity inversion lines, indicative of the complex magnetic configurations that store huge amounts of free magnetic energy and helicity. The challenge is to transform this empirical knowledge into parameters/predictors that can help us distinguish efficiently between quiet, flare-, and CME-productive (eruptive) active regions. This paper reviews these efforts to parameterize the characteristics of eruptive active regions as well as the importance of transforming new knowledge into more efficient predictors and including new types of data. Magnetic properties of active regions were first introduced when systematic ground-based observations of the photospheric magnetic field became possible and the relevant research was boosted by the provision of near real time, uninterrupted, high-quality observations from space, which allowed the study of large, statistically significant samples. Nonetheless, flare and CME prediction still faces a number of challenges. The magnetic field information is still constrained at the photospheric level and accessed only from one vantage point of observation, thus there is always need for better predictors; the dynamic behavior of active regions is still not fully incorporated into predictions; the inherent stochasticity of flares and CMEs renders their prediction probabilistic, thus benchmark sets are necessary to optimize and validate predictions. To meet these challenges, researchers have put forward new magnetic properties, which describe different aspects of magnetic energy storage mechanisms in active regions and offer the opportunity of parametric studies for over an entire solar cycle. This inventory of features/predictors is now expanded to include information from flow fields, transition region and coronal spectroscopy, data-driven modeling of the coronal magnetic field, as well as parameterizations of dynamic effects from time series. Further work towards these directions may help alleviate the current limitations in observing the magnetic field of higher atmospheric layers. In this task, fundamental and operational research converge, with promising results which could stimulate the development of new missions and lay the ground for future exploratory studies, also profiting from and utilizing the long anticipated observations of the new generation of instruments.

## 1 Introduction

Solar flares are sudden, localized brightenings of the solar atmosphere evident throughout the entire electromagnetic spectrum [Fletcher et al., 2011, Shibata and Magara, 2011]. They can release energy in excess of  $10^{25}$  J, within minutes, via both thermal and non-thermal processes. Coronal mass ejections (CMEs) are expulsions of solar coronal plasma into the interplanetary space with velocities that can be as high as  $3500 \text{ km s}^{-1}$  and mass and energy of the order of  $10^{12}$  kg and  $10^{25}$  J, respectively [Chen, 2011, Webb and Howard, 2012]. Flares are categorized in a logarithmic scale according to their soft X-ray emission in the  $1 - 8 \text{ \AA}$  range, as recorded by the Geostationary Operational Environmental Satellites (GOES). From strongest to weakest these classes are X, M, C, B, and A, complemented by

decimal subclasses (M1.0, C5.2, etc.). Flares of M1.0 and higher are often termed major flares, due to their severe impact on space weather. The association between flares and CMEs is not trivial. Statistically, the percentage of flares associated with CMEs increases with the strength of the flare, with the strongest X-class flares almost always associated with a CME [Yashiro et al., 2005]. There are, however, differences in the reported percentages, depending on the solar cycle and the instrument/method of detection [Lamy et al., 2019]. A flare associated with a CME is called eruptive, otherwise, it is a confined flare. The term solar eruption usually describes eruptive flares and the associated CMEs. Both flares and CMEs are facets of the solar activity, usually originating from strong, extended, and often complex magnetic structures called active regions.

Flares and CMEs can affect the space near Earth in many ways, and these effects can occur within minutes, hours and/or days. The enhanced X-ray and EUV emission affect immediately the electron density in a range of ionospheric altitudes, disrupting radio communications, while the subsequent expansion of the atmosphere increases the drag on low-altitude satellites. The direct electromagnetic emission and the energetic particles, which are accelerated in situ and/or by CME fronts are hazardous to space-borne instrumentation and crew and can severely damage infrastructure (space-borne and ground-based), disrupting communications, navigation systems, and power grids [see e.g., Tsurutani et al., 2009, Kontogiannis et al., 2016, Balasis et al., 2019, Daglis et al., 2019].

Understanding these phenomena and mitigating their consequences on space-borne and ground-based infrastructures translates to understanding the mechanisms behind flares and CMEs and to developing efficient prediction schemes. Although the fundamental physics is arguably known [Priest and Forbes, 2002], the specific mechanisms still lack understanding and our ability to predict solar eruptions remains limited. Part of the current research has focused on the evolution of active regions, their characterization with respect to flaring and CME activity and the study of specific mechanisms that lead to these eruptive phenomena.

Active regions store enormous amounts of magnetic energy, which is transformed to the thermal and non-thermal components of solar eruptions via complex magnetic interactions and is more than enough to power solar eruptions. Both for understanding purposes as well as for prediction, the pre-eruptive evolution of active regions is parameterized through properties derived from photospheric vector and/or line-of-sight magnetograms. Some of these properties can be proxies of physical quantities, such as the total unsigned magnetic flux, the vertical current density, the free energy and the helicity. Others characterize the compactness and complexity of active regions, emphasize the presence of strong magnetic field gradients and polarity inversion lines (PILs) or distil information relevant to physical processes such as emergence of magnetic flux and/or shearing motions. The statistical association of these (mostly but not always) magnetic properties with eruptivity has been demonstrated in various samples of flaring and non-flaring regions and their efficiency (or performance) varies per study and sample.

The relevant research flourished with the launch of the Solar Dynamics Observatory [SDO; Pesnell et al., 2012], when a flow of near real-time constant quality photospheric vector magnetograms of active regions was provided by the Helioseismic and Magnetic Imager [HMI; Scherrer et al., 2012]. To further support research and operation, the HMI team issues the Space Weather HMI Active Region Patches (SHARPs), cut-outs of vector magnetograms of regions of interest (such as active regions), along with a set of predictors suitable for space-weather research [Bobra et al., 2014]. This type of data enabled the study of large, statistically significant samples with machine learning (ML) and thus advanced the prediction of flares, the verification of forecasting schemes and the ranking of magnetic properties of the source regions [see e.g., Bobra and Couvidat, 2015, Bobra and Itonidis, 2016, Florios et al., 2018, to name but a few].

Several reviews already exist regarding the properties of flare and CME-productive active regions and the mechanisms that lead to eruption, both from a theoretical and an observational point of view [Schrijver, 2009, Green et al., 2018, Toriumi and Wang, 2019, Patsourakos et al., 2020]. The aim of this review is to present the progress made so far in quantifying the eruptive potential of active regions. This task largely consists in the transformation of a vague notion of complexity into classes and parameters; it was initially based on white light observations, but during the past two decades has relied mostly on photospheric magnetograms, while recently a plethora of EUV observations has also ignited interest in this type of data. More sophisticated parameters are being constructed, aiming to include information relevant to the upper atmosphere and temporal evolution. It is a field of research at the interface between fundamental and operational research, since the derived quantities are crucial

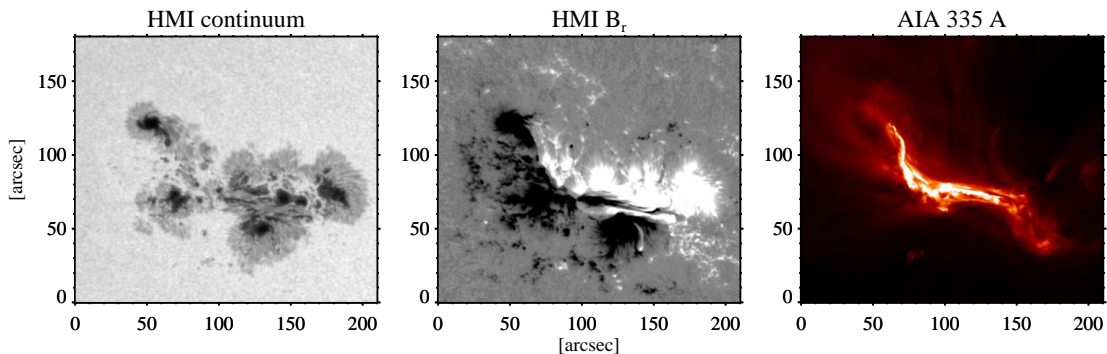


Figure 1: Active region NOAA 11429 as seen on 6 March 2012. From left to right are the continuum at the Fe I 6173 Å, recorded by the HMI, the corresponding map of the radial component of the photospheric magnetic field in the local frame of reference and the intensity at 335 Å recorded by the Atmospheric Imaging Assembly onboard the SDO. This region presented some of the most typical characteristics of highly-eruptive active regions, i.e.,  $\delta$ -spot configuration, strong shearing motions, and a sigmoid seen in coronal EUV/Soft X-ray images. Courtesy of NASA/SDO and the AIA and HMI science teams.

for forecasting services, but can also offer insight into the mechanisms that dictate the pre-eruptive evolution of active regions. It is, therefore, hoped that the works presented here will provide a useful background and also inspire new methodologies, in this era of new solar observations. The reader can find complementary information regarding other crucial aspects of the methodology used in operational flare forecasting in Florios et al. [2018], Leka et al. [2019a,b], Park et al. [2020].

The paper is structured as follows: In Section 2 the characterization of active regions based on ground based observations is discussed, with emphasis on white-light observations. Section 3 reviews the magnetic properties of flaring and erupting active regions, which largely quantify their non-potentiality. After a brief presentation of fractal and multifractal measures in Section 4, the paper then provides a detailed account of recent efforts to produce new properties, mostly, but not exclusively, magnetic. Section 6 is dedicated to efforts on pinpointing those properties that are most suitable for CME prediction, while Section 7 reviews research on quantifying the temporal evolution of active regions and how this information could be incorporated in their prediction. Section 8 summarizes and discusses the progress on characterizing flaring and erupting active regions.

## 2 Quantifying the white-light morphology of active regions

Figure 1 shows a snapshot of active region NOAA 11429, one of the most flare- and CME-productive regions of Solar Cycle 24. It appeared already well-developed on the visible solar limb on 2 March 2012 and produced many flares as it traversed the solar disk. Most notable events were the two consecutive X-class flares produced during the first hours of March 7. As is most often the case with X-class flares, they were associated with fast CMEs, with pronounced effects on the geospace [Patsourakos et al., 2016]. Active region NOAA 11429 exhibited clearly some of the most typical characteristics of flare-productive regions: it had an anti-Hale orientation, i.e., the leading polarity was the positive one, contrary to what expected for the northern hemisphere during that solar cycle; it was exhibiting strong shear along the PIL; in EUV images of the corona it showed sigmoid structures, indicative of a pre-eruptive flux rope [Chintzoglou et al., 2015].

Active region NOAA 11429 exhibited also another typical characteristic of flare-prolific regions, that is a  $\delta$ -spot, i.e., well-developed, opposite polarity sunspots sharing the same penumbra. This descriptor was introduced by Künzel [1965] and it is now used to complement the Mount Wilson (or Hale) classification of sunspots. The original Mount Wilson classification scheme was put forward by Hale [Hale et al., 1919] and it was based on optical, ground-based, white-light and spectropolarimetric observations of active regions. The classes of Mount Wilson categorize sunspot groups in terms of the apparent distribution of their magnetic polarities. Four categories,  $\alpha$ ,  $\beta$ ,  $\beta\gamma$  and  $\gamma$  represent unipolar, bipolar, complex bipolar and irregular/multipolar regions. If the sunspot group contains a  $\delta$ -spot (which, by definition, cannot happen for an  $\alpha$ -type) it can be a  $\beta\delta$ ,  $\gamma\delta$  or  $\beta\gamma\delta$ , depending on the

overall morphology of the active region.

Although based on ground-based observations, the Mount Wilson classification requires information on the magnetic polarity of the sunspots. However, after decades of regular monitoring of the Sun, the white-light-only morphology of the most eruptive active regions had also been noted. These observations are the easiest and the longest, practically available since the era of Galileo and the first scholars, who used the telescope for solar observations, initially in the form of drawings and then, with the development of photography as photographic plates. The benefits of such observations are further appreciated today, since they span many solar cycles and facilitate the association of the number of sunspots and morphology with other aspects of solar activity and observed effects. Automated forecasting systems are based on categorization of these morphological characteristics and parameterizations, derived from large sample. The McIntosh classification system [McIntosh, 1990] offered such a basis and its development was already dictated by the need to improve the statistical association of flare occurrences with discrete classes of active region complexity.

Initially, the classification scheme of Zurich comprised nine classes of white-light complexity, denoted with letters from A to J (I omitted) based on typical evolutionary aspects of the largest sunspot groups [Cortie, 1901, Waldmeier, 1938]. This system was modified to introduce two more classification criteria, namely the morphology of the penumbra of the largest sunspot (indicated by the letters x,r,s,a,h, and k) and the distribution of sunspots within the group (indicated by the letters x,o,i,c). Additionally, it was realized that some of the original Zurich classes (G and J) were redundant in the new scheme, thus leading to an expansion of the remaining seven out of the original Zurich classes into sixty. Although lacking magnetic field information, this classification is more detailed than the Mount Wilson scheme, also incorporating evolutionary aspects, which are missing from the latter. For example, classes at the extremes of the McIntosh scale, such as Axx or Hrx may correspond to  $\alpha$ -type, Bxo or Dsi can be  $\beta$ , while the compact and complex classes, like *Ekc*, *Eki*, *Fkc*, *Eki* correspond to Mount Wilson types with the  $\delta$ -identifier. In fact, the latter categories are associated with the highest M- and X-class flaring rates, as demonstrated in McIntosh [1990].

The McIntosh [1990] study showed the importance of context observations and large statistical samples in establishing the crucial characteristics of flare-productive regions. To this end, the digitization of such observations may expand this sample of observations as far back as the 18<sup>th</sup> century [See Pal et al., 2020, for a non-exhaustive but informative review of digitization efforts]. Moreover, the study also showed that the association between flare-productivity and active region characteristics is statistical: even though it is clear that the most complex classes are associated with higher flaring rates, flares may occur in simpler regions irrespective of the phase of their evolution. This statistical association effectively renders the prediction of flares probabilistic, and transforming probabilities to binary forecasts requires carefully designed validation strategies, as demonstrated in Bloomfield et al. [2012]. The probabilistic nature of flare and CME prediction has persisted and is not expected to change. What has, in fact, changed so far are the data sources, the sophistication of quantifying morphological and magnetic complexity and an increasing trend of reliance on ML for the prediction models.

### 3 Magnetic field parameters

The increasing access to good quality photospheric magnetograms during the 1990's, brought about by the development of ground-based and space-borne instruments facilitated the detailed studies of the magnetism in active regions and its evolution. Exploratory studies were establishing the important role of complexity, size, and rapid emergence of magnetic flux or cancellation in flare-productive regions. Additionally, it was possible to measure physical magnitudes and proxies thereof, i.e., quantities representative of these mechanisms and of the accumulation of magnetic energy in active regions.

A series of landmark papers by Leka and Barnes [2003a,b], Barnes and Leka [2006], Leka and Barnes [2007] illustrated the potential of using such magnetic field-related quantities in solar flare prediction. They used photospheric vector magnetograms acquired by the University of Hawai'i Imaging Vector Magnetograph, from which they calculated several magnetic parameters. The most rudimentary is related to the magnitude of the magnetic field vector and/or its components, measured at each pixel. Since the magnetic field flux density is a signed quantity, its net and total unsigned value can be calculated, as well as its sign imbalance. Vector magnetograms can be used to calculate the inclination angle of the field at the photosphere.

The current instrumentation allows the determination of the magnetic field only at the photosphere, which imposes limitations to the physical magnitudes that can be derived. It is possible to determine the horizontal gradient of the magnetic field, which is a proxy of the compactness of the active region and, thus, [Leka and Barnes \[2003a\]](#) argue that it quantifies the sunspot distribution component of the McIntosh classification. In a similar fashion, one can also calculate (only) the vertical component of the electric current density, which can be treated similarly to the magnetic field density, thus determining the total (net) and the total unsigned electric current, as well as the total value per sign and per magnetic polarity. These parameters are proxies of the energy stored in the current-carrying magnetic field and the net currents injected into the corona.

The product of the vertical magnetic field density and the vertical electric current,  $J_z B_z$ , is used as a proxy of the current helicity, whereas the ratio between the vertical current density and the vertical magnetic flux density is a proxy of the twist of the magnetic field. The twist can also be determined by using the vertical component of the magnetic field as a boundary condition and calculating the linear force-free magnetic field at the photosphere [see e.g., [Alissandrakis, 1981](#)], thus producing one twist value representative for the entire field of view. Similarly, performing an electric current-free (potential) field extrapolation, a proxy of the free magnetic energy density can be derived as the square of the difference between the observed and the potential magnetic fields. It is noted here in passing that a reliable determination of the free magnetic energy is sensitive to measurement errors, to the flux imbalance of the studied region (if any) and the assumptions made regarding the force free magnetic field [see e.g., [Georgoulis and LaBonte, 2007](#), [Georgoulis et al., 2012a](#)]. Additionally, the angle between the two magnetic field vectors is a proxy of the shear angle, which can be calculated on a pixel-by-pixel basis. From this distribution of values, the total/average value for the entire FOV or for regions of interest (such as along PILs) can be determined. Another parameter implemented in these studies was the length of the neutral line (or PIL) for which the shear angle was higher than a specific value (e.g.,  $45^\circ$ ).

For the quantities that were calculated on a pixel-by-pixel basis, in addition to averages, net values and unsigned totals, the higher-order moments of their distributions were also used, namely, the standard deviation, skewness and kurtosis. It was argued that all flare-related mechanisms, e.g., flux emergence, flux cancellation, shearing and twisting (which could lead to an increase in the horizontal components) would produce an observable effect on the related quantities.

The predictors described above were introduced and studied for a limited sample of events and active regions in [Leka and Barnes \[2003a\]](#). The same set of predictors was then extracted from a larger set of observations and discriminant analysis was performed to examine the efficiency of these parameters in discriminating flaring from non-flaring regions [[Leka and Barnes, 2003b](#)].

The characteristic of these quantities is that they are derived from photospheric magnetograms and they are related strictly to the magnetic field state at the photosphere. However, we know that the processes that lead to flares and CMEs take place above the chromosphere. To include quantities relevant to the connectivity and the state of the magnetic field in the corona [Barnes and Leka \[2006\]](#) employed a magnetic charge topology model [[Barnes et al., 2005](#)]. Using a flux tessellation method, the photospheric magnetograms were segmented into non-overlapping unipolar partitions, representing the traces of magnetic charges. This ensemble of partitions was then used to determine a series of topological quantities, such as the number of null points, the separators and their length, the connectivity matrix, the magnetic flux associated with the connections, the magnetostatic energy of the collection of magnetic charges, etc. Discriminant analysis on a small set of events showed the prospect of using MCT-related parameters and in the last paper of the series [[Leka and Barnes, 2007](#)], the array of parameters derived from the photospheric vector magnetograms was tested on a large sample of events.

Other studies focused on specific aspects of the magnetic field non-potentiality. Building on the knowledge that CMEs are produced preferentially by regions with sigmoids, i.e., S-shaped structures seen in some EUV wavelengths and soft X-rays, and that these structures partly outline strong and highly sheared PILs, [Falconer \[2001\]](#) examined the associated CME productivity with two related parameters extracted from vector magnetograms. They calculated the length of strong-field, strong-shear, main neutral line,  $L_{SS}$ , and the net vertical electric current,  $I_N$ , as measures of the global non-potentiality of the studied regions. In a subsequent work [[Falconer et al., 2002](#)] they included also the twist parameter, i.e., the ratio between the vertical electric current and magnetic flux densities. In order to facilitate the use of the line-of-sight magnetograms recorded from both the ground and by the



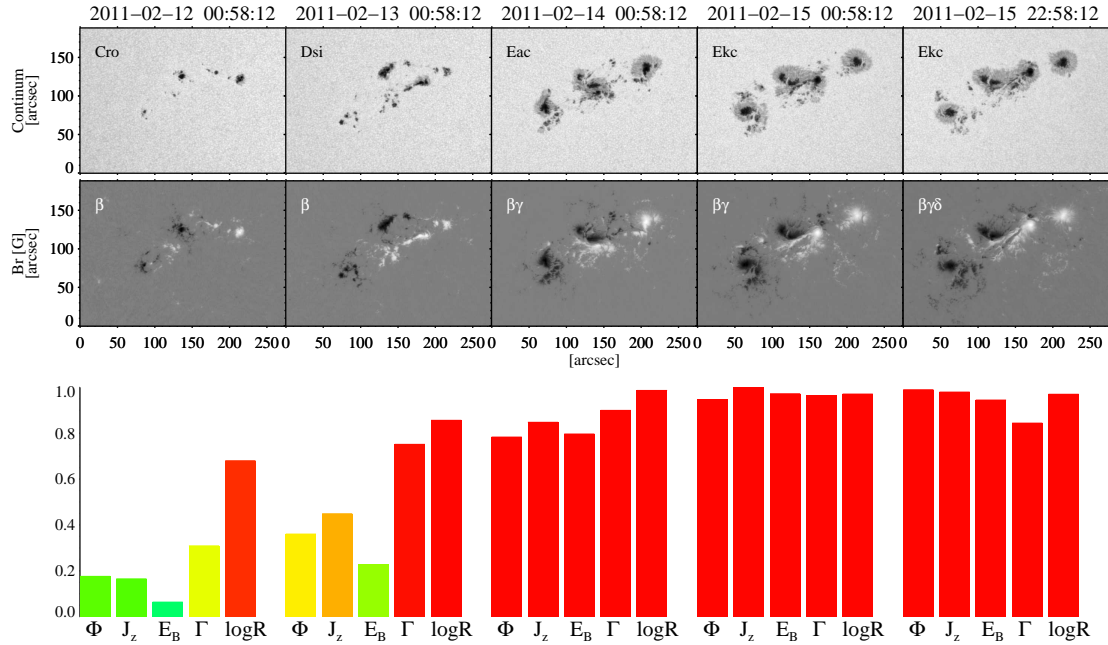


Figure 2: The evolution of NOAA 11158 in McIntosh and Mount Wilson classes as well as in terms of the instantaneous values of some magnetic parameters. The chosen parameters were the total unsigned magnetic flux,  $\Phi$ , the vertical component of the total unsigned electric current density,  $J_z$ , the total photospheric magnetic free energy density,  $E_B$ , the mean shear angle,  $\Gamma$ , and Schrijver's  $R$ . All parameters are included in the SHARP data product and for the purposes of this figure they have been scaled between their minimum and maximum value over the interval between 2011-02-10 21:58 and 2011-02-15 22:58. Courtesy of NASA/SDO and the AIA and HMI science teams. McIntosh and Mount Wilson classes were taken from [solarmonitor.org](http://solarmonitor.org).

Michelson Doppler Imager [MDI; Scherrer et al., 1995] onboard the Solar and Heliospheric Observatory, they developed a proxy for the PIL that could be derived only from the line-of-sight component of the photospheric magnetic field, called  $L_{SG}$  [Falconer et al., 2003]. This was then calculated for an extended set of ground-based magnetograms and it was compared with other non-potentiality measures derived from vector magnetograms [Falconer et al., 2006]. For the PIL-related parameters introduced in these studies only the regions where the shear (for  $L_{SS}$ ) or the horizontal gradient (for  $L_{SG}$ ) were higher than specific thresholds were taken into account. For active regions with many PILs the same authors developed generalized versions of  $L_{SS}$  and  $L_{SG}$ , namely the  $WL_{SS}$  and  $WL_{SG}$ , which were the gradient-weighted integral length of strong shear neutral lines calculated from vector and LOS magnetograms [Falconer et al., 2008a]. These were found to be correlated with the free magnetic energy of active regions and thus they are now used as its proxies in the MAG4 flare-prediction service (<https://www.uah.edu/cspar/research/mag4-page/>).

Having established that PILs are telltale signs of imminent intense flaring activity, several parameterizations were put forward around the same era. Based on the empirical fact that strong flares are observed in the vicinity of PILs, Schrijver [2007] introduced the quantity  $R$ , also called “Schrijver’s  $R$ ”. The PILs are located using morphological image processing and  $R$  is the total unsigned magnetic flux in a 15 Mm-wide region along the PIL. In principle the decimal logarithm of the quantity is being used ( $\log R$ ). For the examined sample of active regions, which spanned from 1999 to 2006, it was found that no major flares (M- or X-class) occurred for regions with  $\log R$  lower than 2.8, but when this value was higher than 5 the flaring probability reached unity. Another morphological quantity introduced to quantify the presence of strong, i.e., highly-sheared, PILs is the effective connected magnetic field strength,  $B_{eff}$  [Georgoulis and Rust, 2007]. This quantity is derived from the connectivity matrix of the partitioned magnetogram [Barnes et al., 2005], and it is the total of the magnetic flux associated with all connections, weighted by their length. This quantity is used in an operational forecasting scheme, the Athens Effective Solar Flare Forecasting (A-EFFORT), which is part of the European Space Agency (ESA) Space Situation Awareness (SSA) Programme. Detection algorithms of PILs such as the one presented in Mason and Hoeksema [2010] can be used to determine more rudimentary characteristics such as the length of the main PIL, the total length of PILs in an active regions and the associated magnetic flux [see also: Guerra et al., 2018], which is similar to Schrijver’s  $R$ . Another measure of the compactness of active regions, called Ising Energy, a term inspired by the Ising model of ferromagnetism in statistical mechanics, was introduced by Ahmed et al. [2010]. This metric is the sum of the inverse square distances between all possible opposite polarity pixel pairs of an active region. A higher number of closely neighboring, opposite polarity magnetic field concentrations, which is typically the case in the presence of strongly sheared PILs and  $\delta$ -spots, will lead to higher values of Ising energy.

Parameters derived from the magnetic field still remain the main features for prediction models. The parameters included in [Leka and Barnes, 2007], along with Schrijver’s  $R$  and  $WL_{SG}$  are included in the list of space weather related parameters of the SHARP data products [Bobra et al., 2014]. This data set spans now more than one full solar cycle and it is invaluable for testing new forecasting schemes. Recently, this data product was extended to include the LOS photospheric magnetograms recorded by the MDI instrument. The Space Weather MDI Active Region Patches [SMARPS; Bobra et al., 2021] effectively extend our inventory of some magnetic parameters over two solar cycles [see also Sun et al., 2022, for an assessment of using two solar cycle data in training prediction models]. It is also worth mentioning that in the context of the recent project Flare Likelihood And Region Eruption Forecasting [FLARECAST; Georgoulis et al., 2021] all available parameters were gathered and calculated for the SHARP cut-outs and comprise the data base of the project, upon which forecasting models were based. The list comprises 209 predictors and includes all the aforementioned quantities, along with those discussed in Section 4 as well as newly developed ones, described in Section 5.

An example of how these magnetic parameters reflect the evolution of active regions is shown in Figures 2 and 3. The top and middle rows of Figure 2 show the evolution of the well-studied active region NOAA 11158, from 12 to 15 February 2011, in terms of overall white light morphology (along with McIntosh classes) and the photospheric longitudinal magnetic field. The region emerged towards the end of February 10 and within a few days it evolved from a relatively simple bipolar region into a  $\delta$ -spot, producing several C- and M-class flares, as well as the first X-class flare of Solar Cycle 24. At the bottom row of Figure 2, the respective morphological evolution is given in terms of five magnetic parameters, namely, the total unsigned magnetic flux,  $\Phi$ , the vertical component of the total unsigned

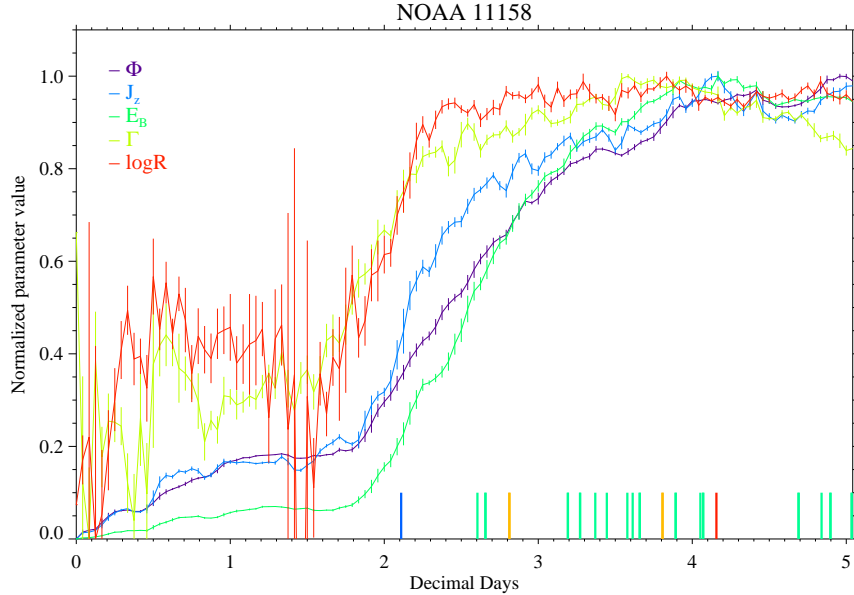


Figure 3: Temporal evolution of the magnetic parameters shown in Figure 2 for NOAA 11158, starting at 2011-02-10 21:58 UT. Blue, green, orange and red vertical lines at the lower part of the plot indicate B-, C-, M-, and X-class flares, correspondingly.

electric current density,  $J_z$ , the total photospheric magnetic free energy density,  $E_B$ , the mean shear angle,  $\Gamma$ , and Schrijver's  $R$ . All parameters are provided with the SHARP data product for NOAA 11158 and here they have been normalized to their minimum (set to 0) and maximum (set to 1) values during the lifetime of this active region and are shown without their units. It is clear how the increase in complexity, both in terms of white-light morphology and magnetic field reflects on the values of all the magnetic parameters. The intensely flaring phase of the region, after February 13, followed the rapid increase of all parameters. In a statistical sense, higher values of these parameters should be associated with higher flaring rates, as is the case in this example.

However, the temporal evolution of the five parameters is not identical since each of them is associated with a slightly different aspect of the region's non-potentiality (size, appearance and development of PIL and shear, etc.). Figure 3 shows the corresponding time series in more detail. The time series have a cadence equal to 1 h, instead of the 12 min cadence originally provided with SHARPs, and are also normalized to their minimum and maximum values. As the active region emerged, the magnetic flux and free energy densities increased slowly during the first two days and then rapidly, as the region entered its intensely flaring phase. The electric current density followed a similar evolution, but with a more steep increase after the second day. The increase in the three parameters persisted until at least the end of the fifth day. The evolution of the mean shear and  $\log R$  exhibits some notable differences. These parameters are most closely associated with PILs, they exhibited some noisy behavior during the initial stages of emergence, when the first bipoles appeared and grew, then diminished as the polarities separated, but increased sharply before the end of the second day when the main PIL formed. The mean shear continued to increase until a few hours before the X-class flare and then decreased, while  $\log R$  was roughly constant during the entire flaring phase of the active region. These differences in evolution may be linked to the specific mechanisms that are responsible for intense flaring, such as strong converging and shearing motions, the development of magnetic shear, the emergence of magnetic flux and flux cancellation, and deserve further attention. In the context of flare prediction they can justify some of the differences regarding the efficiency of some parameters, the assessment of which depends on sample selection and prediction method.



## 4 Fractal and multifractal properties

The visual complexity of the photospheric magnetic field of active regions and their evolution towards critical states and destabilization have inspired their study in terms of their fractal and turbulent properties. In these cases the distribution of the magnetic field with values higher than a specific threshold is treated as an irregular shape whose fractal dimension can be determined. Since not only the spatial distribution, but also the values of the magnetic field may exhibit fractal properties, one can also examine the fractal properties of the distribution for varying indices and magnetic field thresholds, thus determining a multifractal spectrum. An account of early studies of the fractal properties of the magnetic field in quiet Sun and in plages, as well as a treatment of the distribution of the magnetic field flux density as a multifractal is given by [Lawrence et al. \[1993\]](#). Since then, a number of studies have investigated the use of fractal measures as predictors of imminent flaring activity.

The simplest measure of the self-similarity of a set (in our case the magnetic field distribution of an active region) is the fractal dimension, which can be most simply determined using box counting. The process consists in covering the mask of the magnetic field distribution with a grid of boxes, counting the number of boxes containing at least one pixel of the mask, and repeating for various sizes of boxes. The number of boxes as a function of size should obey a power law, whose index is the fractal dimension. In principle, the fractal dimension of both the active region area and its boundary can be determined using the same method. [McAteer et al. \[2005\]](#) applied the box-counting technique to a set of more than 9000 full-disk MDI magnetograms, and reported a tendency for flaring active regions to exhibit fractal dimension higher than 1.2.

The multifractal measures take into account the values of the magnetic field distribution. The corresponding methods result in the determination of a multifractal spectrum, from which specific indices may be used as predictors. The formalism to calculate the multifractal spectra of magnetic fields, in terms of generalized correlation dimensions and/or Hölder exponents and Hausdorff dimensions is described in [Lawrence et al. \[1993\]](#). A series of studies have explored the connection between multifractal dimensions and flare productivity [e.g., [Georgoulis, 2005](#), [Conlon et al., 2008](#), [Hewett et al., 2008](#), [Ireland et al., 2008](#), [Criscuoli et al., 2009](#), [Giorgi et al., 2015](#)] and report a different behavior of the multifractal spectra and the values of specific multifractal dimensions of intensely flaring active regions.

Another way to investigate the intermittency and turbulence present in a magnetic field distribution is through the multifractal structure function spectrum. [Abramenko et al. \[2002\]](#) studied the scaling behavior of the LOS magnetograms of four active regions with different flaring activity. The structure functions are equivalent to the correlation functions of a vector field (in this case the magnetic field) and are calculated as the statistical moments of the field increments, over a grid of separation vectors within the FOV. The range of separation vectors is defined as the inertial range. The structure functions follow power laws whose scaling indices can be determined through fitting.

An assessment of the potential of fractal and multi-fractal parameters in flare prediction was attempted by [Georgoulis \[2012\]](#) and [Georgoulis \[2013\]](#), for a representative sample of active regions observed by MDI and two case-studies of emerging active regions exhibiting different activity, observed by HMI, correspondingly. It was concluded that multi-scale parameters do not seem to provide a better chance of predicting flares than other fundamental or proxy parameters related to the non-potentiality of active regions. The latter study also highlights two important aspects of characterizing the non-potentiality of active regions, namely that it is possible to create more sophisticated proxy parameters to improve flare prediction and that the temporal evolution of the proxy and fundamental parameters need also be taken into account to this end. In Sections 5 and 7, recent efforts towards these two directions are reviewed.

## 5 Searching for new predictors

The easy access to high-quality, near-real-time, photospheric magnetograms and context EUV coronal imaging for over a decade now, the accumulation of new and digitization of older synoptic observations, combined with the increasing concern about the implications of solar storms have further fueled research on improved prediction metrics and methods. One aspect of this research was the search for more efficient parameterizations of the pre-eruptive state of active regions, both in strictly magnetic and in non-magnetic terms.

In a series of papers, [Korsós et al. \[2014, 2015\]](#), [Korsós and Erdélyi \[2016\]](#) proposed a new way to measure the horizontal gradient of the magnetic field, based on white light observations. They argued that white-light images would suffer less than photospheric magnetograms from the geometric foreshortening effects, which affect observations away from the solar disk center and that these could be easily corrected using simple transforms. They used simultaneous observations of sunspot groups and photospheric magnetograms close to the solar disk center to calibrate the umbrae areas into magnetic field values. With this calibration relation at hand, they calculated the horizontal gradient of the magnetic field as the sum of all differences between the areas of opposite-polarity umbrae, weighted by the average separation distance between the leading and trailing polarities. Following their work on the photospheric horizontal magnetic gradient, they suggested its extension at higher atmospheric layers, with the aid of extrapolations of the magnetic field [[Korsós et al., 2020a](#)]. The methodology put forward by [Korsós et al. \[2015\]](#) was applied to a sample of  $\sim 10000$  SHARP cut-outs by [Kontogiannis et al. \[2018\]](#) who also did a preliminary assessment of the efficiency of horizontal gradient in comparison with other new predictors. Additionally, combining elements from the methodology of [Korsós et al. \[2015\]](#) and [Barnes et al. \[2005\]](#), they introduced two new variations of the Ising energy [[Ahmed et al., 2010](#)], namely, the Ising energy of the magnetic partitions  $E_{Ising,part}$  and the Ising energy of sunspot umbrae  $E_{Ising,spot}$ . These quantities were calculated in a similar manner as the original, but instead of opposite polarity pixel they considered opposite polarity partitions/umbrae. It was then demonstrated that both new quantities as well as the horizontal gradient,  $G_S$ , had increased potential as predictors.

Based on the method of calculating the amount of net currents injected to the corona suggested by [Georgoulis et al. \[2012b\]](#), two new predictors were introduced by [Kontogiannis et al. \[2017\]](#), namely, the total unsigned non-neutralized electric current,  $I_{NN,tot}$  and the maximum non-neutralized current  $I_{NN,max}$ . These were tested in a sample of active regions and also  $\sim 10000$  SHARP cut-outs and it was found that their values correlated well with the flare productivity of active regions and exhibited higher flaring rates than other commonly used electric current-related parameters.

The difference between  $I_{NN,tot}$  and the vertical component of the electric current density,  $J_z$  is shown, for two active regions with different flaring activity, in [Figure 4](#). Both parameters followed a similar trend as the active regions evolved. However, the values of the  $I_{NN,tot}$  were lower than  $J_z$  by roughly one order of magnitude (note that the time series in [Figure 4](#) were normalized to facilitate comparison), because the latter is calculated from the entire distribution of the magnetic field vector (within a bitmap mask) whereas the former only from the non-neutralized partitions. As per the proposed methodology, these are the magnetic partitions for which the electric current density is significantly higher than the erroneous numerical or error-propagated electric currents. These criteria, chosen by [Georgoulis et al. \[2012b\]](#), ensure that only neighboring partitions which have developed sheared PILs contribute to the value of  $I_{NN,tot}$ , whereas isolated magnetic partitions should, in principle, be neutralized and not contribute to the calculation. This important difference makes the relation between  $J_z$  and  $I_{NN,tot}$ , non-trivial, since for simple active regions  $I_{NN,tot}$  is zero while  $J_z$  is not. As seen in [Figure 4](#), the correlation coefficients between the two parameters calculated for the two active regions clearly differ. For NOAA 11072 the correlation is moderate (0.52) since most of the partitions of the region are neutralized. For NOAA 11158, the correlation is almost unity (0.98), since the region developed intense shearing motions as it evolved, leading to a similar increase in  $I_{NN,tot}$ . In fact, the strong correlation between the two parameters is due to the evolution observed after the second day of its emergence. Therefore, during this phase in the overall evolution of the active region the increase in  $J_z$  is due to electric current injected to the corona by the non-neutralized partitions. On the contrary, this is not the case during the first two days: although  $J_z$  increases monotonically following the growth of the region, this is not the case for  $I_{NN,tot}$ , as a result of low shear and absence of strong PILs during the early stage of the emergence. The association between non-neutralized electric currents and strongly sheared PILs is further discussed in [Georgoulis et al. \[2012b\]](#) and [Kontogiannis et al. \[2017, 2019\]](#), while more work is underway, but this example illustrates how exploratory research can lead to more refined predictors, i.e., parameters that reflect in more detail the specifics of the mechanisms that lead to flares and CMEs.

Before discussing some alternative ways to utilize observations to derive predictors of flaring activity, it is worth mentioning that this research can also be aided by scrutiny of simulations. [Guennou et al. \[2017\]](#) tested and developed some non-potentiality metrics and assessed their ability to differentiate between eruptive and non-eruptive numerical setups using numerical experiments of flux emergence instead of observations. Along with the importance of the parameters introduced by [Falconer et al.](#)

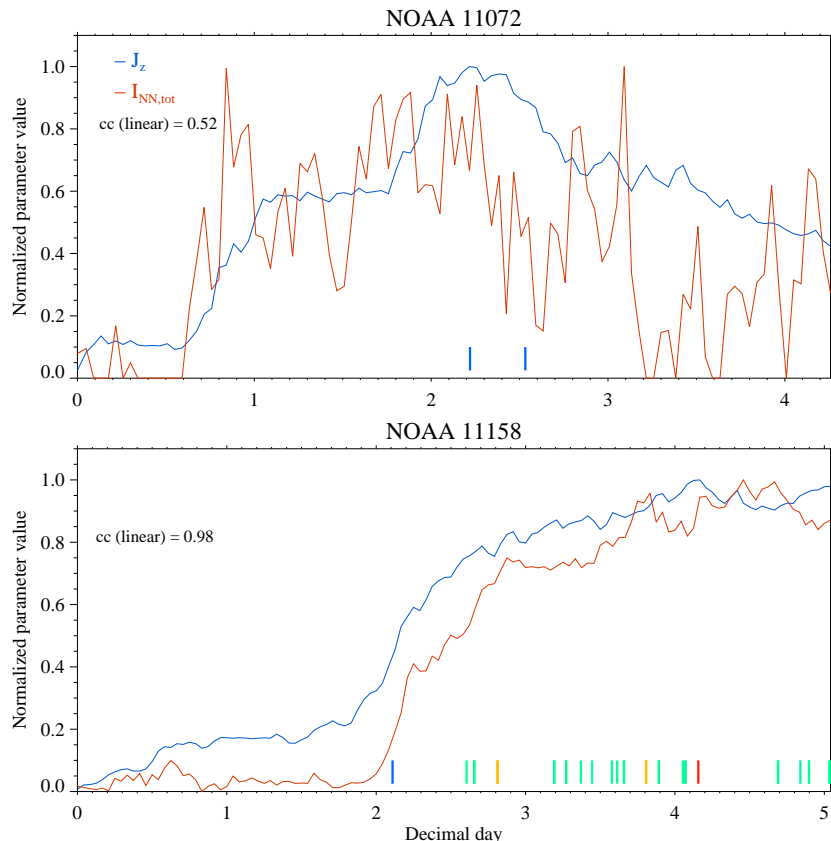


Figure 4: The evolution of the vertical component of the total unsigned electric current density (blue) and the total unsigned non-neutralized electric current (red) for active regions NOAA 11072 (top) and 11158 (bottom), from the start of their emergence at 2010-05-20 16:22 and 2011-02-10 21:58 UT correspondingly. The two time series are scaled to their maximum values to facilitate comparison. Blue, green, orange and red vertical lines indicate B-, C-, M-, and X-class flares, respectively.

[2008b], they also highlighted the efficiency of new parameters, such as the length of the strong-current MPIL and the corresponding integral of the magnetic field along it.

Another aspect of active region evolution is relevant to the observed photospheric proper motions and flow fields. Welsch et al. [2009] used Fourier Local Correlation Tracking (FLCT) and the Differential Affine Velocity Estimator [DAVE; Schuck, 2005] to extract the flow fields from MDI active region observations. Then they produced an array of quantities to parameterize the flow fields in order to investigate their association with flaring activity. The list included quantities related to the magnetic field, the flow field, their moments, the divergence and convergence close to the PIL, Schrijver’s R, etc. They noted that their proxy of the Poynting flux, i.e., the sum of the product of flow velocity and square radial magnetic field was the one with the strongest association with flare flux. Park et al. [2018] used the Differential Affine Velocity Estimator for Vector Magnetograms [DAVE4VM; Schuck, 2008] to measure the flow fields of a large sample of flaring and non-flaring active regions observed by HMI. Their focus was on the shear flows along the PIL and, thus, three quantities were constructed, namely, the mean, total (integral) and maximum along the PIL, as well as the corresponding horizontal and vertical flow speeds. Although all parameters show similar trends with flaring activity, their results suggest that a measure of the shear flows such as the integral along the MPIL could be used in flare prediction. The conclusion from these two works is that the flow field information in active

region could be incorporated in the prediction of flares and CMEs, although more work is required.

The increasing abundance of high quality EUV context and spectroscopic observations of active regions in the UV have facilitated the study of sizeable samples. In this context, [Panos and Kleint \[2020\]](#) gathered Mg II h & k lines spectra of active regions observed by the Interface Region Imaging Spectrograph [IRIS [De Pontieu et al., 2014](#)]. The spectra were represented in terms of ten spectral parameters (intensity, Doppler shift, line width, asymmetry, continuum, triplet emission at the red wing, k/h ratio, k3 intensity, peak ratios and peak separation), all of them reflecting physical conditions up to the chromosphere. They used both unsupervised - Principal Component Analysis (PCA) and t-distributed stochastic neighbor embeddings (t-SNE) - and supervised (neural networks) ML and concluded that the triplet emission, followed by intensity and total continuum were the leading parameters. Further utilization of non-magnetic information was done by [Gontikakis et al. \[2020\]](#), who formulated parameters based on the Differential Emission Measure (DEM) of active regions, as reconstructed by AIA imaging. They used data provided by the Gaussian AIA DEM maps [GAIA-DEM; [Guennou et al., 2012a,b](#)] provided by the Multi Experiment Data & Operation Center (MEDOC; <https://idoc-medoc.ias.u-psud.fr/>). The database contains maps of four parameters, namely, the emission measure (i.e. the temperature integral of the DEM curve), the maximum temperature and width of the DEM distribution (corresponding to the position of maximum and the width of the fitted Gaussian), as well as the  $\chi^2$  of the fit. They demonstrated that the temporal derivative of the emission measure and the maximum temperature can be used to forecast flares, especially for shorter forecast windows. An additional interesting aspect of the aforementioned works on flow fields and the DEM-related parameters is that the proposed predictors also contain information on the dynamical evolution of the active regions.

During the past few years some different methods to parameterize active region complexity have been developed. [Deshmukh et al. \[2020\]](#) used topological analysis to construct the persistence diagrams of magnetograms using different magnetic flux thresholds and then transformed these into vectors, which they used as predictors to train ML algorithms. Additionally, they implemented geometrical features such as the number and size of positive (negative) elements, their average distance as well as the interaction factor, a measure similar to the Ising energy. They trained a neural network with the geometrical and topological features, complemented with the SHARP parameters and concluded that the new predictors could improve forecasts. [Sun et al. \[2021\]](#) also included features derived from topological analysis, such as variograms, along with their different versions of SHARP parameters. Since the classical SHARP parameters represent total or average values over a region around the active region, they produced modifications of these parameters by placing more weight on the region around the PIL, following the method of [Wang et al. \[2020\]](#). Additionally, they employed spatial statistics tools such as Ripley's K function and variograms to quantify the clustering of pixels above specific magnetic flux density thresholds. Then, through a PCA they kept the top five components from each K function and topological features and concluded that the corresponding features perform equally well and sometimes better than the SHARP parameters.

[Cicogna et al. \[2021\]](#) parameterized PILs using a topological descriptor called  $D$ , which represents the number of PIL fragments in an active region. The opposite polarity fragments were detected using thresholding, segmentation and labeling of the LOS magnetograms. They used  $D$  along with a version of Schrijver's  $R$  and the properties extracted by the forecasting engine of FLARECAST [[Georgoulis et al., 2021](#)]. They reported that  $D$  was always included in the top-10 performing predictors in all realizations of the forecasting scheme. [Raphaldini et al. \[2022\]](#) suggested a new metric called magnetic winding as a proxy of the magnetic helicity. The quantity was calculated without the need of three-dimensional extrapolations of the magnetic field and relied on the decomposition of the magnetic field into potential and current-carrying components. They presented five examples of flaring and non-flaring active regions to illustrate the potential of the new metric.

Finally, instead of calculating complexity parameters, abstract characteristics can be extracted from magnetograms. For instance, [Raboonik et al. \[2017\]](#) and [Alipour et al. \[2019\]](#) used the Zernike moments of cut-outs of the active region magnetograms and EUV filtergrams as features for flare prediction. Another way to quantify the complexity and eruptive potential of active regions is to directly feed magnetograms or filtergrams into ML algorithms [see e.g., [Wang et al., 2019](#), [Jonas et al., 2018](#), [Nishizuka et al., 2021](#), [Abed et al., 2021](#)].

## 6 Quantifying the potential to erupt: parameters suitable for CME prediction

Although the standard solar model or eruptions [also referred to as the CSHKP model, from the initials of Carmichael, 1964, Sturrock, 1966, Hirayama, 1974, Kopp and Pneuman, 1976] and its subsequent revisions describe both flares and CME’s as aspects of a single eruptive process, the two phenomena are not always associated, as already discussed in the introduction. Although CMEs from active regions are always associated with flares, the opposite is not necessarily true. The study and prediction of flares have been prioritized for historical reasons, since they were discovered more than a century earlier than CMEs and for years they were considered to be the primary aspect of solar activity. This has now changed but there are also practical reasons for this “bias”: while there is often enough time to model and predict the effects of CMEs upon their detection in white-light coronagraphic observations, the impact of flares is immediate. Nevertheless, the adverse effects of CMEs to geospace also call for accurate forecasting schemes. One way to accomplish this is to find which parameters are more effective for CME prediction, that is, which of them can help effectively distinguish eruptive from non-eruptive flares. An extra step is to modify some of the already existing parameters or even produce new ones, to improve their association with eruptions. Towards this direction, and given the fact that magnetic parameters are relevant mostly to the photospheric magnetic field, some recent studies have started to incorporate more elaborate information aiming to include the role of the constraining magnetic field.

The phenomenology of solar eruptions is described by the standard model in terms of a core field, either a magnetic flux rope [Titov and Démoulin, 1999] or a sheared arcade [van Ballegooijen and Martens, 1989], which is constrained by an overlying magnetic field. This two-dimensional model has been updated to accommodate observational aspects in three dimensions, such as the formation of sigmoids, flare ribbons with J-shaped ends and changes in the 3D configuration of the magnetic field before and after the eruptions [Aulanier et al., 2012, 2013, Janvier et al., 2013]. The process described by the standard model requires a triggering mechanism, which will produce an unstable configuration, and drivers which will initiate the eruption [see Green et al., 2018, for a comprehensive review of the theoretical descriptions that have been put forward so far].

In this context, two quantities are of interest regarding CME initiation, the magnetic helicity and the decay index. The magnetic helicity [Berger and Field, 1984] is a measure of the degree of linkage, twist, and writhe of the magnetic field lines and accumulates as the active regions emerge and build up free magnetic energy [see e.g. Tziotziou et al., 2012, 2013]. As a quantity, the magnetic helicity is conserved during dissipative processes but it is removed from active regions during eruptions. Its properties make it crucial in understanding the triggering mechanisms of CMEs as there are indications that when certain thresholds of free magnetic energy and helicity are exceeded, an eruption is initiated [e.g., see discussion in Georgoulis et al., 2019]. Thus, proxies of the instantaneous budget and accumulation rate of magnetic helicity have received attention as possible predictors of eruptions [Park et al., 2010, 2012, Georgoulis, 2013, Georgoulis et al., 2021]. On the other hand, the decay index, which is derived from magnetic field extrapolations, describes how fast the constraining magnetic field decays and, thus, determines whether a full eruption could take place or not [Török and Kliem, 2005, Liu, 2008, Zuccarello et al., 2014, 2015]. A faster decrease, i.e., higher decay index, reflects more favourable conditions for eruption. Based on the aforementioned works, three predictors based on the decay index were developed by the FLARECAST consortium [Georgoulis et al., 2021], namely the mean value of the decay index above PILs, the height at which the decay index reaches 1.5 and the ratio between this height and the length of the PIL.

From the studies already mentioned in Section 3, the ones by Falconer et al. [2006] and Falconer et al. [2008a] have specifically addressed the prediction of CMEs. They highlighted the importance of twist and free energy in CME-productive active regions and their non-potentiality as represented by the  $WL_{SG}$ , that is, the gradient-weighted length of the neutral lines in an active region. More recently, Vasantharaju et al. [2018] demonstrated how calculating known parameters along manually tracked PILs can improve the correlation between magnetic parameters and CME characteristics.

The issue of determining which magnetic parameters are more suitable for CME prediction was tackled through machine learning by Bobra and Itonidis [2016], for a sample of SHARP data. In their work they discussed the distinction between extensive and intensive magnetic characteristics, and concluded that the latter are the most important for CME prediction. Extensive characteristics are the ones that scale with the size of the active region, such as the total magnetic flux, the total



electric current density, and other “total” quantities. On the other hand, parameters that do not scale with the active region size, such as average quantities or quantities relevant to specific source region features such as PILs, etc. are non-extensive or intensive. In this context, quantities like,  $B_{eff}$ ,  $\log R$ ,  $WLSG$ , but also  $I_{NN,tot}$  are intensive, since they correspondingly emphasize the presence of PILs, represent the magnetic flux in their vicinity, quantify their length or are proxies of the net electric currents injected to the corona.

Aiming to further explore the relevance of such PIL-related quantities, [Kontogiannis et al. \[2019\]](#) gathered a sample of 32 active regions/events of Solar Cycle 24 and calculated ten predictors, including some widely used ( $R, WLSG, B_{eff}$ ) and recently introduced ones ( $I_{NN,tot}, I_{NN,max}, E_{Ising}, E_{Ising,part}, E_{Ising,spot}$ , the length of PIL and the associated magnetic flux). The predictors were calculated along an interval of 24h before eruption and their daily-averaged values were correlated with kinematic characteristics of eruptions. It was found that the total unsigned non-neutralized electric currents and the length of the PIL were the ones most strongly correlated with CME characteristics, whose correlations improved when only the fastest events were considered. Their results were largely in line with earlier studies [[Pal et al., 2018](#)], but also demonstrated the relationship between net electric currents and strongly sheared PILs as well as their potential use in CME prediction.

Lacking detailed measurements of the coronal magnetic field vector, some new parameters have attempted to include information relevant to the magnetic field in higher atmospheric layers using data-driven modelling. [Pagano et al. \[2019a\]](#) derived the parameters  $\zeta$  from a data-driven magnetofrictional model, which incorporates information on the existence of magnetic flux-ropes and the Lorentz force. The eruption metric  $\zeta$  is space- and time-dependent and can give information on the location of the eruption, while its maximum value, averaged over the entire time series of magnetograms can be used to distinguish eruptive from non-eruptive regions. In a follow-up study [[Pagano et al., 2019b](#)] they elaborated their method and produced the quantity  $\Lambda$ , which they derived from the distribution of  $\zeta$ , as a more suitable parameter for operational forecasting of CMEs. [Lin et al. \[2020\]](#) applied non-linear force-free field (NLFFF) extrapolation to determine the twist of the magnetic field lines and discriminate between the core and the ambient magnetic fields. They produced the parameter  $r_m$ , i.e., the ratio of the magnetic flux associated with high twist to that of the overlying magnetic flux. However, they reported a moderate predictive potential of the proposed quantity (a relative measure of the core and constraining magnetic field), because further information from flare ribbons was required to pinpoint flare locations. [Li et al. \[2022\]](#) calculated the twist in regions close to the PIL and then divided the twist parameters with the total magnetic flux of the active region, which they consider representative of the constraining magnetic field. They concluded that the new parameter could distinguish effectively, for the examined sample, the eruptive from the non-eruptive cases.

## 7 Quantifying the temporal evolution of active regions

In the vast majority of the studies discussed so far, the formulated magnetic parameters were encapsulating a point-in-time information and thus represented a static condition in the evolution of active regions. However, active regions evolve dynamically and it is exactly the nature of this evolution that leads to major events [[Georgoulis et al., 2019](#)]. The quantities used as predictors offer the chance to study the evolution of active regions in terms of their non-potentiality, revealing evolutionary patterns and mechanisms in action. Indeed, several exploratory studies on the development of non-potentiality in eruptive active regions have reported specific pre-eruptive patterns.

The systematic provision of good quality LOS magnetograms by MDI facilitated the study of the helicity injection rate in flaring active regions [[Kusano et al., 2002](#), [LaBonte et al., 2007](#), see e.g.], which showed that major flares followed specific threshold values of helicity and long intervals of increase. [Park et al. \[2008\]](#) found that before 11 X-class flares the magnetic helicity underwent a two-phase evolution: a monotonic accumulation, followed by a constant phase. The rate of helicity accumulation was more strongly correlated with the soft X-ray flux than the amount of helicity itself. Although the rate of helicity injection itself was not sufficient to describe the helicity history of an active region, flaring regions exhibited statistically twice as high helicity injection rate [[Park et al., 2010](#)]. The pre-eruptive behavior of NOAA 11158 was studied by [Tziotziou et al. \[2013\]](#) in terms of free energy and magnetic helicity. [Georgoulis \[2013\]](#) further studied the evolution of the same region in terms of the effective connected magnetic field strength,  $B_{eff}$ , and compared it with that of multi-scale parameters. The pre-eruptive evolution of the horizontal gradient proxies introduced by [Korsós et al.](#)

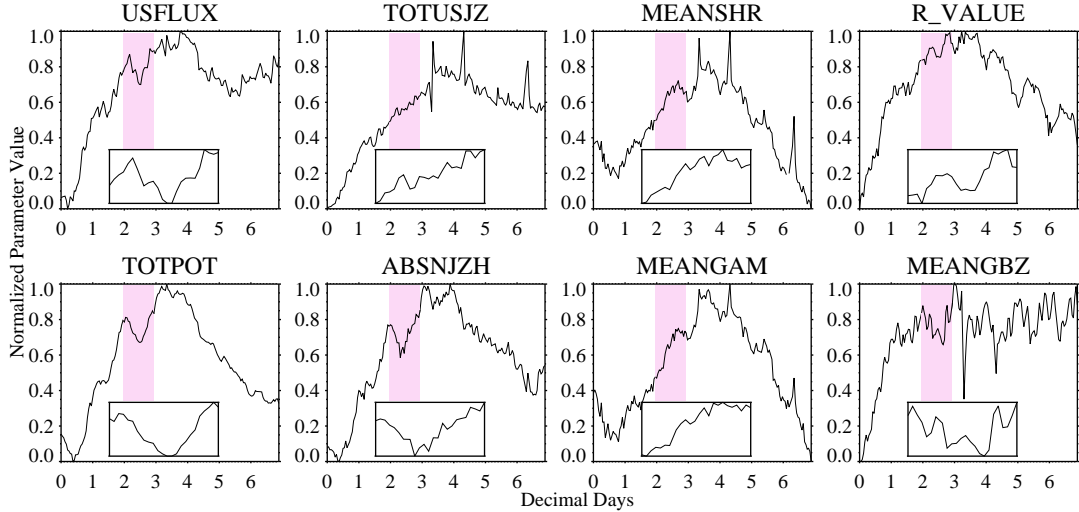


Figure 5: Temporal evolution of eight SHARP parameters for active region NOAA 11429. From top left to right bottom, these parameters are the total unsigned magnetic flux, the total unsigned vertical electric current density, the shear angle, Schrijver’s  $\log R$ , the total photospheric magnetic free energy density proxy, the absolute value of the net current helicity, the mean angle of field from radial direction, and the mean horizontal gradient of the vertical magnetic field. The insets show the evolution of the same parameters during the 24h before the twin X-class flares of 7 March 2012 (shaded with lilac in the original plots). All parameters are normalized to their minimum and maximum values, as in previous figures.

[2014, 2015] were studied for a few active regions indicating a specific evolutionary pattern before major flares. Other non-potentiality metrics such as the non-neutralized electric currents and the Ising energy exhibited structure with distinct peaks before major flares [Kontogiannis et al., 2017, 2018]. Kontogiannis et al. [2019] showed that, within the 24 hours that preceded eruptions, different parameters exhibited different temporal evolution; the correlation of the parameters values with the characteristics of CMEs could increase if, instead of daily averages one considered instantaneous values on specific times before the events. Recently, Korsós et al. [2020b] examined, for a limited sample of  $\delta$ -spot active regions, the periodicities of the magnetic helicity injection rate, which they decomposed into the emergence and the shearing term. They noticed that the most flare-productive ones shared a common periodic behavior. Soós et al. [2022] extended the analysis to a balanced set of 28 active regions, and reported that the emergence term of the magnetic helicity injection rate in flaring regions (i.e., those that hosted X-class flares) exhibited mostly shorter period oscillations (shorter than 10h) a few hours prior to X-class flares. However, in both studies no discussion of the origin of these oscillations was provided. This non-exhaustive account of studies and results attests to the wealth of information contained in the temporal evolution of the magnetic characteristics of active regions. Recent studies have started to incorporate them into flare prediction, utilizing the almost uninterrupted provision of photospheric magnetograms from HMI for more than one solar cycle.

The evolution of eight SHARP parameters for active region NOAA 11429 is shown in Figure 5. As also discussed for NOAA 11158 (Figure 3), these parameters follow a generally similar trend, but with differences regarding their overall steepness of increase and the existence of distinct peaks. Additionally, as demonstrated by Kontogiannis et al. [2018] different parameters have different sensitivity on instrumental and geometric effects. Focusing on the evolution of these parameters during the day before the X-class flare of 7 March 2012 (insets in the panels of Figure 5, it is well seen that some parameters exhibit an almost monotonic increase until the onset of the event, while others show clear peaks and valleys. While this is only one example, it is reasonable to inquire whether specific parameters exhibit a systematic behavior, how this behavior can be quantified and what is its importance to flare and CME prediction.

Before reviewing how temporal information of magnetic parameters has been incorporated to predictions, it is worth noting that the flaring history of active regions itself has been shown to be a

good indicator of future activity. [Wheatland \[2005\]](#) described a methodology wherein the probabilities of future GOES events (particularly strong ones) can be inferred using the distributions of prior ones. The flaring history is routinely included as an extra feature in explored and operational forecasting schemes and is often found to be one of the top performers [[Falconer et al., 2014](#), [Liu et al., 2019](#), [Leka et al., 2019a,b](#), [Park et al., 2020](#)].

Regarding dynamic effects, so far these have been incorporated into predictions in two ways. One of them is to use entire time series of predictors to train machine learning models. In this case the temporal information already contained in the time series is utilized, without this having been quantified with specific parameters [see e.g., [Huang et al., 2010](#), [Yu et al., 2010a,b](#), [Chen et al., 2019](#), [Liu et al., 2020](#)]. The other strategy is to extract features related to the history of active regions, either their past flaring activity or the trend exhibited by their complexity parameterizations. Usually, this requires the choice of time intervals, over which the statistics of the flare history will be calculated or features like derivatives or summary characteristics will be extracted.

[Lee et al. \[2012\]](#) included also the change in the white-light area, as an indicator of flux emergence or cancellation. They did so by complementing the McIntosh classes with three additional categories, depending on the direction of area change, namely “decrease”, “steady” and “increase”. They noted that higher probability rates were associated with increasing area. [McCloskey et al. \[2018\]](#) proposed a forecasting scheme based on the evolution of complexity of active regions. They did so by calculating the flaring rates associated with the change of McIntosh classes over 24 h intervals. Evolution towards class of higher complexity was associated with higher flaring rates and validation and bias correction for the differences across solar cycles indicated an improved performance for the forecast based on the McIntosh evolution.

Aiming to include measures of the existence and intensity of magnetic flux emergence [Al-Ghraibah et al. \[2015\]](#) introduced nine flux-emergence-related features. To calculate these features they subtracted subsequent magnetograms and isolated the regions that stood above a  $3\sigma$  difference level. From this they calculated the sum (net and absolute), the area and the statistics (mean, standard deviation, minimum and maximum over the mask). Additionally, they used this  $3\sigma$  mask to calculate the gradient of the second image. Their feature space, consisting both of static (magnetic and fractal-related) and temporal (flux-emergence-related) parameters was then used to train Regression Vector Machines and, in a follow-up study, Support Vector Regression models [[Boucheron et al., 2015](#)]. Their results support the overall discriminatory power of the predictor ensemble to classify flaring and non-flaring events but no conclusion on the importance of the temporal parameters was drawn. [Nishizuka et al. \[2017\]](#) trained three ML algorithms using features extracted from magnetograms and EUV images of active regions. These features included also temporal derivatives of features and the flaring history, as recorded by GOES. The latter was deemed an important feature that improved flare prediction in their model. Although the point-in-time values of magnetic parameters were found overall more important than their differentials, concerning the latter, the derivatives calculated over 24 h were found more important than those over shorter intervals.

[Leka et al. \[2018\]](#) described the Discriminant Analysis Flare Forecasting System (DAFFS) of the North Western Research Associates (NWRA). Along with the standard predictors introduced in their earlier work, the scheme included also previous flaring information and magnetic parameter time series information. The latter was introduced by modelling 6 hour-long time-series’ segments with a linear function. The time-series segments end on the time of the issuing of the forecast. The derived slope and intercept were treated as predictors. Although the previous flaring information is among the top performing predictors, the inclusion of the preceding temporal variation of the magnetic parameters in the form of slope and intercept did not lead to a notable improvement in the forecasts, even though they could contribute to equally competent predictions. It should be noted in passing that various combinations of the many parameters utilized by [Leka et al. \[2018\]](#) performed similarly well, within the error margins.

[Lee et al. \[2018\]](#) used a Detrended Fluctuation Analysis to remove persistent patterns and quantify the random variations in consecutive non-overlapping segments of time series. The detrended fluctuation and the time series averages were positively correlated with the imminent 8-day flare index. In a follow-up study [Lee et al. \[2020\]](#) found that flaring regions exhibited higher values of the scaling exponent of the detrended fluctuations. [Pauker et al. \[2019\]](#) used spline interpolation on segments of time series, and then utilized the spline coefficients as additional predictors, along with standard ones, which lead to a slight improvement of predictions.

Notwithstanding different strategies and approaches, and despite still lacking a definitive assessment on the improvement of predictions when incorporating time series, their importance is generally accepted. Current facilities/instruments not only provide ample data but also facilitate the construction of standardized multivariate time series datasets for further studies. [Angryk et al. \[2020\]](#) created such a benchmark data product, which comprises time series of selected magnetic properties and, most importantly, an “error-free” association with flare occurrences. Data sets like this provide a test bed to compare different approaches, not only for prediction models based on time series but also for those relying on point-in-time information.

A more in-depth exploration of characteristic patterns in large statistical samples is still missing and such a task could benefit both exploratory and operational research. Time-series based operational forecasting of flares and CMEs can not be realized without standardized, continuous observations of the Sun. Since it takes at least a few days of observations to produce a times series of magnetic parameters, the current instrumentation limits forecasts only for the regions closer to the central meridian. Therefore, the capabilities of incorporating time series in forecasts can be fully exploited in the future if continuous observations from different vantage points complement the existing ones, offering access to active regions before they rotate into the earth-facing side of the Sun [[Vourlidis, 2015](#)].

## 8 Summary and outlook

The increased awareness of national/international space agencies and stakeholders on the adverse consequences of space weather [[Schrijver et al., 2015](#)] has fueled fundamental and operational research in the relevant fields of heliophysics. This fact reflects on the abundance of studies on space weather prediction during the past decade. Before and up to the 1990’s studies were limited by the limited available observations; during the past two decades a multitude of instruments provided access to many facets of solar activity, from the emergence of new magnetic flux on the solar surface to influences seen on outer corona, solar wind and interplanetary space. Nowadays, at least in solar physics, it is perhaps hard to imagine how research would be without the standard flow of continuous, high-quality magnetic field measurements and coronal imaging provided by missions like SDO.

Consequently, flare and CME prediction has moved forward by creating an inventory of active region characteristics and prediction methods. The characteristics (predictors or parameters) amass to more than two hundred [see e.g., [Georgoulis et al., 2021](#)] and incorporate quantities relevant mostly to the photospheric magnetic field, but highlight different aspects, such as size, various physical quantities (electric current, magnetic energy, magnetic helicity) and proxies thereof, PIL characteristics and connectivity. Regarding the prediction methods, these are now dominated by ML, with increasing sophistication on sample selection and validation. The community is working intensely towards comparing methods and setting standards, which will help provide the most accurate possible forecasts and address the needs of interested parties [see e.g., [Barnes et al., 2016](#), [Leka et al., 2019a,b](#), [Park et al., 2020](#)].

Notwithstanding the access to large, high-quality statistical samples and sophisticated methods, the prediction of solar eruptions remains probabilistic, due to the nature of solar eruptions and the limitations of observations. Flares are inherently stochastic, in the sense that given favourable conditions, they may happen at any time and the available free energy can be channeled in any combination of flare magnitudes and CME energetics, producing one major event, several smaller ones or both. Furthermore, the characteristics of flare- and CME-productive active regions are relevant to the photosphere, despite the fact that the magnetic interactions that power solar eruptions take place  $\gtrsim 2$  Mm higher. It is, therefore, reasonable that the magnetic parameters exhibit a degree of redundancy and that there is also no conclusive answer on which single parameter can provide the best results. This has been already highlighted by [Leka and Barnes \[2007\]](#), who showed that the inclusion of many properties does not necessarily improve the forecast, and more recently by [Campi et al. \[2019\]](#), who also concluded that the inherent stochasticity of flares does not allow a binary (i.e. “yes/no”) forecast.

On the other hand, it is largely supported that probabilistic forecasts can improve when using better data sources and methods [[Leka et al., 2019a](#)]. Since no systematic provision of coronal magnetic field observations is expected in the immediate future, one course of action is to continue searching for improved predictors based on the data provided by current instrumentation. The studies cited in this review show how results from fundamental research can be transformed into promising new

predictors, corroborating that there is indeed still room for improvement in quantifying aspects of imminent eruptive activity. New properties now incorporate more sophisticated information from image processing, photospheric flow fields, spectroscopy and data-driven modelling, the last two of which are, at the moment, our only way to probe higher atmospheric layers. On the one hand, spectra and observables from transition region and the corona provide information more relevant to the atmospheric layers where the initiation of flares and CMEs takes place, with promising future implications [Judge et al., 2021]. On the other hand, data-driven modelling, although it cannot fully compensate for our lack of coronal magnetic field measurements, is our only way to probe the three-dimensional vector magnetic field in the solar atmosphere and assess the competing roles of the core and ambient magnetic field in CME initiation [Amari et al., 2018]. Further work is required here to instill this information into more refined parameters and advance CME prediction.

Finally, there is a growing body of work on exploiting the dynamic behavior of active regions, utilizing the, now abundant, time series of existing magnetic properties. Moving from the “static” point-in-time treatment of source regions to monitoring their entire evolution from emergence to decay is a huge leap forward for the relevant fields of research. Some of this dynamic information is incorporated into prediction schemes. Nowadays ML offers a huge variety of methods to treat time-series, for knowledge discovery, classification and/or prediction [Bagnall et al., 2017] and it is up to the community to proceed towards this direction in a more systematic way, especially given the availability of openly accessible, standardized datasets [Angryk et al., 2020].

To the authors experience, a common question is how new missions, like the Solar Orbiter [Müller et al., 2020] and the new generation of ground-based solar telescopes, such as the Daniel K. Inouye Solar Telescope [DKIST; Rimmele et al., 2020] and the European Solar Telescope [EST; Quintero Noda et al., 2022], can contribute to the task of flare and CME prediction. A short response would be that they cannot, since statistically significant samples of standardized, continuous observations are necessary to transform any systematic behavior into parameters suitable for prediction and to test their potential efficiency. They are, however, expected to contribute indirectly by enhancing our understanding of solar eruptive phenomena and pointing to specific connections between solar drivers and space weather effects. This was the case with Hinode and IRIS missions. Although they were not intended for operational space research they did contribute to characterizing the potential of active regions to erupt, either by igniting further research [Georgoulis et al., 2012a, Harra et al., 2013, Syntelis et al., 2016] or, eventually, by directly producing sizeable samples of observations [Panos and Kleint, 2020]. Therefore, it is expected that those new facilities and instrumentation will stimulate further fundamental research and open new windows in solar observation, particularly by supplying accurate measurements of the magnetic field at higher atmospheric layers.

A final note is reserved here for the important role of big projects like FLARECAST [Georgoulis et al., 2021]. The efficient prediction of flares, CMEs and other space weather aspects rely on a gamut of techniques and (sub-)fields. These include solar and space physics, computer science, and machine learning, complemented by outreach, which is necessary to coordinate communication with interested parties, raise awareness and stimulate citizen science projects. Therefore, critical elements for such a task are interdisciplinarity and collaboration between communities and stakeholders. FLARECAST brought together experts from these areas to produce a novel flare-prediction service. By gathering all available parameters and implementing new ideas, not only it created a comprehensive set of magnetic parameters but also enriched it with new, promising ones. It is expected that such an accomplishment will serve as a prototype for future endeavours and also ignite new ways to characterize the flaring and eruptive potential of solar active regions.

## 9 Acknowledgments

I would like to thank the two anonymous reviewers for providing detailed and constructive comments, which significantly improved the content and presentation of this paper. I would also like to thank the Scientific Organizing Committee of the 16<sup>th</sup> European Solar Physics Meeting (ESPM-16), for the invitation to present a review on the topic presented in this paper. I.Kontogiannis is supported by KO 6283/2-1 of the Deutsche Forschungsgemeinschaft (DFG). For this paper, data from SDO/AIA, SDO/HMI and particularly SHARP were used. These are courtesy of NASA/SDO and the AIA, EVE, and HMI science teams and are publicly available through the Joint Science Operations Center at the [jsoc.stanford.edu](http://jsoc.stanford.edu). Part of the calculations was performed using source codes made publicly



available by the H2020 project FLARECAST (<https://dev.flarecast.eu/stash/projects/>).

## References

- L. Fletcher, B. R. Dennis, H. S. Hudson, S. Krucker, K. Phillips, A. Veronig, M. Battaglia, L. Bone, A. Caspi, Q. Chen, P. Gallagher, P. T. Grigis, H. Ji, W. Liu, R. O. Milligan, and M. Temmer. An Observational Overview of Solar Flares. *Space Sci. Rev.*, 159:19–106, September 2011. doi: DOI:10.1007/s11214-010-9701-8.
- K. Shibata and T. Magara. Solar Flares: Magnetohydrodynamic Processes. *Living Rev. Solar Phys.*, 8:6, December 2011.
- P. F. Chen. Coronal Mass Ejections: Models and Their Observational Basis. *Living Reviews in Solar Physics*, 8(1):1, April 2011. doi: 10.12942/lrsp-2011-1.
- D. F. Webb and T. A. Howard. Coronal Mass Ejections: Observations. *Living Reviews in Solar Physics*, 9:3, June 2012. doi: DOI:10.12942/lrsp-2012-3.
- S. Yashiro, N. Gopalswamy, S. Akiyama, G. Michalek, and R. A. Howard. Visibility of coronal mass ejections as a function of flare location and intensity. *Journal of Geophysical Research (Space Physics)*, 110(A12):A12S05, December 2005. doi: 10.1029/2005JA011151.
- P. L. Lamy, O. Floyd, B. Boclet, J. Wojak, H. Gilardy, and T. Barlyaeva. Coronal Mass Ejections over Solar Cycles 23 and 24. *Space Sci. Rev.*, 215(5):39, August 2019. doi: 10.1007/s11214-019-0605-y.
- B. T. Tsurutani, O. P. Verkhoglyadova, A. J. Mannucci, G. S. Lakhina, G. Li, and G. P. Zank. A brief review of “solar flare effects” on the ionosphere. *Radio Science*, 44(A5):RS0A17, July 2009. doi: 10.1029/2008RS004029.
- Ioannis Kontogiannis, Anna Belehaki, Georgia Tsiropoula, Ioanna Tsagouri, Anastasios Anastasiadis, and Athanasios Papaioannou. Building a new space weather facility at the National Observatory of Athens. *Advances in Space Research*, 57(1):418–430, January 2016. doi: 10.1016/j.asr.2015.10.028.
- G. Balasis, C. Papadimitriou, and A. Z. Boutsis. Ionospheric response to solar and interplanetary disturbances: a Swarm perspective. *Philosophical Transactions of the Royal Society of London Series A*, 377(2148):20180098, July 2019. doi: 10.1098/rsta.2018.0098.
- Ioannis A. Daglis, Christos Katsavrias, and Marina Georgiou. From solar sneezing to killer electrons: outer radiation belt response to solar eruptions. *Philosophical Transactions of the Royal Society of London Series A*, 377(2148):20180097, July 2019. doi: 10.1098/rsta.2018.0097.
- E. R. Priest and T. G. Forbes. The magnetic nature of solar flares. *Astron. Astrophys. Rev.*, 10(4): 313–377, January 2002. doi: 10.1007/s001590100013.
- W. Dean Pesnell, B. J. Thompson, and P. C. Chamberlin. The Solar Dynamics Observatory (SDO). *Solar Phys.*, 275(1-2):3–15, January 2012. doi: DOI:10.1007/s11207-011-9841-3.
- P. H. Scherrer, J. Schou, R. I. Bush, A. G. Kosovichev, R. S. Bogart, J. T. Hoeksema, Y. Liu, T. L. Duvall, J. Zhao, A. M. Title, C. J. Schrijver, T. D. Tarbell, and S. Tomczyk. The Helioseismic and Magnetic Imager (HMI) Investigation for the Solar Dynamics Observatory (SDO). *Solar Phys.*, 275: 207–227, January 2012. doi: DOI:10.1007/s11207-011-9834-2.
- M. G. Bobra, X. Sun, J. T. Hoeksema, M. Turmon, Y. Liu, K. Hayashi, G. Barnes, and K. D. Leka. The Helioseismic and Magnetic Imager (HMI) Vector Magnetic Field Pipeline: SHARPs - Space-Weather HMI Active Region Patches. *Solar Phys.*, 289:3549–3578, September 2014. doi: DOI:10.1007/s11207-014-0529-3.
- M. G. Bobra and S. Couvidat. Solar Flare Prediction Using SDO/HMI Vector Magnetic Field Data with a Machine-learning Algorithm. *Astrophys. J.*, 798(2):135, January 2015. doi: 10.1088/0004-637X/798/2/135.

- M. G. Bobra and S. Ilonidis. Predicting Coronal Mass Ejections Using Machine Learning Methods. *Astrophys. J.*, 821(2):127, April 2016. doi: 10.3847/0004-637X/821/2/127.
- Kostas Florios, Ioannis Kontogiannis, Sung-Hong Park, Jordan A. Guerra, Federico Benvenuto, D. Shaun Bloomfield, and Manolis K. Georgoulis. Forecasting solar flares using magnetogram-based predictors and machine learning. *Solar Phys.*, 293(2):28, 2018. doi: DOI:10.1007/s11207-018-1250-4.
- Carolus J. Schrijver. Driving major solar flares and eruptions: A review. *Advances in Space Research*, 43(5):739–755, March 2009. doi: 10.1016/j.asr.2008.11.004.
- Lucie M Green, Tibor Török, Bojan Vršnak, Ward Manchester, and Astrid Veronig. The Origin, Early Evolution and Predictability of Solar Eruptions. *Space Science Reviews*, 214(1):46, February 2018. doi: DOI:10.1007/s11214-017-0462-5.
- Shin Toriumi and Haimin Wang. Flare-productive active regions. *Living Reviews in Solar Physics*, 16(1):3, May 2019. doi: 10.1007/s41116-019-0019-7.
- S. Patsourakos, A. Vourlidas, T. Török, B. Kliem, S. K. Antiochos, V. Archontis, G. Aulanier, X. Cheng, G. Chintzoglou, M. K. Georgoulis, L. M. Green, J. E. Leake, R. Moore, A. Nindos, P. Syntelis, S. L. Yardley, V. Yurchyshyn, and J. Zhang. Decoding the Pre-Eruptive Magnetic Field Configurations of Coronal Mass Ejections. *Space Sci. Rev.*, 216(8):131, November 2020. doi: 10.1007/s11214-020-00757-9.
- K. D. Leka, Sung-Hong Park, Kanya Kusano, Jesse Andries, Graham Barnes, Suzy Bingham, D. Shaun Bloomfield, Aoife E. McCloskey, Veronique Delouille, David Falconer, Peter T. Gallagher, Manolis K. Georgoulis, Yuki Kubo, Kangjin Lee, Sangwoo Lee, Vasily Lobzin, JunChul Mun, Sophie A. Murray, Tarek A. M. Hamad Nageem, Rami Qahwaji, Michael Sharpe, Robert A. Steenburgh, Graham Steward, and Michael Terkildsen. A Comparison of Flare Forecasting Methods. II. Benchmarks, Metrics, and Performance Results for Operational Solar Flare Forecasting Systems. *Astrophys. J. Suppl. Ser.*, 243(2):36, Aug 2019a. doi: DOI:10.3847/1538-4365/ab2e12.
- K. D. Leka, Sung-Hong Park, Kanya Kusano, Jesse Andries, Graham Barnes, Suzy Bingham, D. Shaun Bloomfield, Aoife E. McCloskey, Veronique Delouille, David Falconer, Peter T. Gallagher, Manolis K. Georgoulis, Yuki Kubo, Kangjin Lee, Sangwoo Lee, Vasily Lobzin, JunChul Mun, Sophie A. Murray, Tarek A. M. Hamad Nageem, Rami Qahwaji, Michael Sharpe, Robert A. Steenburgh, Graham Steward, and Michael Terkildsen. A Comparison of Flare Forecasting Methods. III. Systematic Behaviors of Operational Solar Flare Forecasting Systems. *Astrophys. J.*, 881(2):101, August 2019b. doi: DOI:10.3847/1538-4357/ab2e11.
- Sung-Hong Park, K. D. Leka, Kanya Kusano, Jesse Andries, Graham Barnes, Suzy Bingham, D. Shaun Bloomfield, Aoife E. McCloskey, Veronique Delouille, David Falconer, Peter T. Gallagher, Manolis K. Georgoulis, Yuki Kubo, Kangjin Lee, Sangwoo Lee, Vasily Lobzin, JunChul Mun, Sophie A. Murray, Tarek A. M. Hamad Nageem, Rami Qahwaji, Michael Sharpe, R. A. Steenburgh, Graham Steward, and Michael Terkildsen. A Comparison of Flare Forecasting Methods. IV. Evaluating Consecutive-day Forecasting Patterns. *Astrophys. J.*, 890(2):124, February 2020. doi: DOI:10.3847/1538-4357/ab65f0.
- S. Patsourakos, M. K. Georgoulis, A. Vourlidas, A. Nindos, T. Sarris, G. Anagnostopoulos, A. Anastasiadis, G. Chintzoglou, I. A. Dagleis, C. Gontikakis, N. Hatzigeorgiu, A. C. Iliopoulos, C. Katsavrias, A. Kouloumvakos, K. Moraitis, T. Nieves-Chinchilla, G. Pavlos, D. Sarafopoulos, P. Syntelis, C. Tsironis, K. Tziotziou, I. I. Vogiatzis, G. Balasis, M. Georgiou, L. P. Karakatsanis, O. E. Malandraki, C. Papadimitriou, D. Odstrčil, E. G. Pavlos, O. Podlachikova, I. Sandberg, D. L. Turner, M. N. Xenakis, E. Sarris, K. Tsinganos, and L. Vlahos. The Major Geoeffective Solar Eruptions of 2012 March 7: Comprehensive Sun-to-Earth Analysis. *Astrophys. J.*, 817(1):14, January 2016. doi: 10.3847/0004-637X/817/1/14.
- Georgios Chintzoglou, Spiros Patsourakos, and Angelos Vourlidas. Formation of Magnetic Flux Ropes during a Confined Flaring Well before the Onset of a Pair of Major Coronal Mass Ejections. *Astrophys. J.*, 809(1):34, August 2015. doi: 10.1088/0004-637X/809/1/34.

- H. Künzel. Zur Klassifikation von Sonnenfleckengruppen. *Astronomische Nachrichten*, 288:177, December 1965.
- George E. Hale, Ferdinand Ellerman, S. B. Nicholson, and A. H. Joy. The Magnetic Polarity of Sun-Spots. *Astrophys. J.*, 49:153, April 1919. doi: 10.1086/142452.
- P. S. McIntosh. The classification of sunspot groups. *Solar Phys.*, 125:251–267, February 1990. doi: DOI:10.1007/BF00158405.
- A. L. Cortie. On the Types of Sun-Spot Disturbances. *Astrophys. J.*, 13:260, May 1901. doi: 10.1086/140816.
- M. Waldmeier. Chromosphärische Eruptionen. I. Mit 6 Abbildungen. *Z. Astrophys.*, 16:276, January 1938.
- Partha S. Pal, Meetu Verma, Jürgen Rendtel, Sergio Javier González Manrique, Harry Enke, and Carsten Denker. Solar observatory Einstein Tower: Data release of the digitized solar full-disk photographic plate archive. *Astronomische Nachrichten*, 341(575):575–587, July 2020. doi: 10.1002/asna.202013791.
- D. S. Bloomfield, P. A. Higgins, R. T. J. McAteer, and P. T. Gallagher. Toward Reliable Benchmarking of Solar Flare Forecasting Methods. *Astrophysical Journal Letters*, 747:L41, March 2012. doi: DOI:10.1088/2041-8205/747/2/L41.
- K. D. Leka and G. Barnes. Photospheric Magnetic Field Properties of Flaring versus Flare-quiet Active Regions. I. Data, General Approach, and Sample Results. *Astrophys. J.*, 595(2):1277–1295, October 2003a. doi: 10.1086/377511.
- K. D. Leka and G. Barnes. Photospheric Magnetic Field Properties of Flaring versus Flare-quiet Active Regions. II. Discriminant Analysis. *Astrophys. J.*, 595(2):1296–1306, October 2003b. doi: 10.1086/377512.
- G. Barnes and K. D. Leka. Photospheric Magnetic Field Properties of Flaring versus Flare-quiet Active Regions. III. Magnetic Charge Topology Models. *Astrophys. J.*, 646(2):1303–1318, August 2006. doi: 10.1086/504960.
- K. D. Leka and G. Barnes. Photospheric Magnetic Field Properties of Flaring versus Flare-quiet Active Regions. IV. A Statistically Significant Sample. *Astrophys. J.*, 656(2):1173–1186, February 2007. doi: 10.1086/510282.
- C. E. Alissandrakis. On the computation of constant alpha force-free magnetic field. *Astron. Astrophys.*, 100(1):197–200, July 1981.
- Manolis K. Georgoulis and Barry J. LaBonte. Magnetic Energy and Helicity Budgets in the Active Region Solar Corona. I. Linear Force-Free Approximation. *Astrophys. J.*, 671(1):1034–1050, December 2007. doi: 10.1086/521417.
- Manolis K. Georgoulis, Kostas Tziotziou, and Nour-Eddine Raouafi. Magnetic Energy and Helicity Budgets in the Active-region Solar Corona. II. Nonlinear Force-free Approximation. *Astrophys. J.*, 759(1):1, November 2012a. doi: 10.1088/0004-637X/759/1/1.
- G. Barnes, D. W. Longcope, and K. D. Leka. Implementing a Magnetic Charge Topology Model for Solar Active Regions. *Astrophys. J.*, 629(1):561–571, August 2005. doi: 10.1086/431175.
- D. A. Falconer. A prospective method for predicting coronal mass ejections from vector magnetograms. *J. Geophys. Res.*, 106(A11):25185–25190, November 2001. doi: 10.1029/2000JA004005.
- D. A. Falconer, R. L. Moore, and G. A. Gary. Correlation of the Coronal Mass Ejection Productivity of Solar Active Regions with Measures of Their Global Nonpotentiality from Vector Magnetograms: Baseline Results. *Astrophys. J.*, 569(2):1016–1025, April 2002. doi: 10.1086/339161.

- P. H. Scherrer, R. S. Bogart, R. I. Bush, J. T. Hoeksema, A. G. Kosovichev, J. Schou, W. Rosenberg, L. Springer, T. D. Tarbell, A. Title, C. J. Wolfson, I. Zayer, and MDI Engineering Team. The Solar Oscillations Investigation - Michelson Doppler Imager. *Solar Phys.*, 162:129–188, December 1995. doi: DOI:10.1007/BF00733429.
- D. A. Falconer, R. L. Moore, and G. A. Gary. A measure from line-of-sight magnetograms for prediction of coronal mass ejections. *Journal of Geophysical Research (Space Physics)*, 108(A10):1380, October 2003. doi: 10.1029/2003JA010030.
- D. A. Falconer, R. L. Moore, and G. A. Gary. Magnetic Causes of Solar Coronal Mass Ejections: Dominance of the Free Magnetic Energy over the Magnetic Twist Alone. *Astrophys. J.*, 644(2): 1258–1272, June 2006. doi: 10.1086/503699.
- D. A. Falconer, R. L. Moore, and G. A. Gary. Magnetogram Measures of Total Nonpotentiality for Prediction of Solar Coronal Mass Ejections from Active Regions of Any Degree of Magnetic Complexity. *Astrophys. J.*, 689(2):1433–1442, December 2008a. doi: 10.1086/591045.
- C. J. Schrijver. A Characteristic Magnetic Field Pattern Associated with All Major Solar Flares and Its Use in Flare Forecasting. *Astrophys. J. Lett.*, 655:L117–L120, February 2007. doi: DOI: 10.1086/511857.
- M. K. Georgoulis and D. M. Rust. Quantitative Forecasting of Major Solar Flares. *Astrophys. J. Lett.*, 661:L109–L112, May 2007. doi: DOI:10.1086/518718.
- J. P. Mason and J. T. Hoeksema. Testing Automated Solar Flare Forecasting with 13 Years of Michelson Doppler Imager Magnetograms. *Astrophys. J.*, 723:634–640, November 2010. doi: DOI:10.1088/0004-637X/723/1/634.
- J. A. Guerra, S. H. Park, P. T. Gallagher, I. Kontogiannis, M. K. Georgoulis, and D. S. Bloomfield. Active Region Photospheric Magnetic Properties Derived from Line-of-Sight and Radial Fields. *Solar Phys.*, 293(1):9, January 2018. doi: 10.1007/s11207-017-1231-z.
- O. Ahmed, R. Qahwaji, T. Colak, T. Dudok De Wit, and S. Ipson. A new technique for the calculation and 3D visualisation of magnetic complexities on solar satellite images. *Visual Comp.*, 26:385–395, February 2010. ISSN 0178-2789. doi: DOI:10.1007/s00371-010-0418-1.
- Monica G. Bobra, Paul J. Wright, Xudong Sun, and Michael J. Turmon. SMARPs and SHARPs: Two Solar Cycles of Active Region Data. *Astrophys. J. Suppl. Ser.*, 256(2):26, October 2021. doi: 10.3847/1538-4365/ac1f1d.
- Zeyu Sun, Monica G. Bobra, Xiantong Wang, Yu Wang, Hu Sun, Tamas Gombosi, Yang Chen, and Alfred Hero. Predicting Solar Flares Using CNN and LSTM on Two Solar Cycles of Active Region Data. *arXiv e-prints*, art. arXiv:2204.03710, April 2022.
- Manolis K. Georgoulis, D. Shaun Bloomfield, Michele Piana, Anna Maria Massone, Marco Soldati, Peter T. Gallagher, Etienne Pariat, Nicole Vilmer, Eric Buchlin, Frederic Baudin, Andre Csillaghy, Hanna Sathiapal, David R. Jackson, Pablo Alingery, Federico Benvenuto, Cristina Campi, Konstantinos Florios, Constantinos Gontikakis, Chloe Guennou, Jordan A. Guerra, Ioannis Kontogiannis, Vittorio Latorre, Sophie A. Murray, Sung-Hong Park, Samuel von Stachelski, Aleksandar Torbica, Dario Vischi, and Mark Worsfold. The flare likelihood and region eruption forecasting (FLARECAST) project: flare forecasting in the big data & machine learning era. *Journal of Space Weather and Space Climate*, 11:39, May 2021. doi: 10.1051/swsc/2021023.
- J. K. Lawrence, A. A. Ruzmaikin, and A. C. Cadavid. Multifractal Measure of the Solar Magnetic Field. *Astrophys. J.*, 417:805, November 1993. doi: 10.1086/173360.
- R. T. James McAteer, Peter T. Gallagher, and Jack Ireland. Statistics of Active Region Complexity: A Large-Scale Fractal Dimension Survey. *Astrophys. J.*, 631(1):628–635, September 2005. doi: 10.1086/432412.
- Manolis K. Georgoulis. Turbulence In The Solar Atmosphere: Manifestations And Diagnostics Via Solar Image Processing. *Solar Phys.*, 228(1-2):5–27, May 2005. doi: 10.1007/s11207-005-2513-4.

- P. A. Conlon, P. T. Gallagher, R. T. J. McAteer, J. Ireland, C. A. Young, P. Kestener, R. J. Hewett, and K. Maguire. Multifractal properties of evolving active regions. *Solar Physics*, 248(2):297–309, Apr 2008. ISSN 1573-093X. doi: DOI:10.1007/s11207-007-9074-7.
- R. J. Hewett, P. T. Gallagher, R. T. J. McAteer, C. A. Young, J. Ireland, P. A. Conlon, and K. Maguire. Multiscale Analysis of Active Region Evolution. *Solar Phys.*, 248:311–322, April 2008. doi: DOI:10.1007/s11207-007-9028-0.
- J. Ireland, C. A. Young, R. T. J. McAteer, C. Whelan, R. J. Hewett, and P. T. Gallagher. Multiresolution Analysis of Active Region Magnetic Structure and its Correlation with the Mount Wilson Classification and Flaring Activity. *Solar Phys.*, 252(1):121–137, October 2008. doi: 10.1007/s11207-008-9233-5.
- S. Criscuoli, P. Romano, F. Giorgi, and F. Zuccarello. Magnetic evolution of superactive regions. Complexity and potentially unstable magnetic discontinuities. *Astron. Astrophys.*, 506(3):1429–1436, November 2009. doi: 10.1051/0004-6361/200912044.
- F. Giorgi, I. Ermolli, P. Romano, M. Stangalini, F. Zuccarello, and S. Criscuoli. The Signature of Flare Activity in Multifractal Measurements of Active Regions Observed by SDO/HMI. *Solar Phys.*, 290(2):507–525, February 2015. doi: 10.1007/s11207-014-0609-4.
- V. I. Abramenko, V. B. Yurchyshyn, H. Wang, T. J. Spirock, and P. R. Goode. Scaling Behavior of Structure Functions of the Longitudinal Magnetic Field in Active Regions on the Sun. *Astrophys. J.*, 577:487–495, September 2002. doi: DOI:10.1086/342169.
- Manolis K. Georgoulis. Are Solar Active Regions with Major Flares More Fractal, Multifractal, or Turbulent Than Others? *Solar Phys.*, 276(1-2):161–181, February 2012. doi: 10.1007/s11207-010-9705-2.
- Manolis K. Georgoulis. Toward an efficient prediction of solar flares: Which parameters, and how? *Entropy*, 15(11):5022–5052, Nov 2013. ISSN 1099-4300. doi: DOI:10.3390/e15115022.
- M. B. Korsós, T. Baranyi, and A. Ludmány. Pre-flare Dynamics of Sunspot Groups. *Astrophys. J.*, 789:107, July 2014. doi: DOI:10.1088/0004-637X/789/2/107.
- M. B. Korsós, A. Ludmány, R. Erdélyi, and T. Baranyi. On Flare Predictability Based on Sunspot Group Evolution. *Astrophys. J. Lett.*, 802:L21, April 2015. doi: DOI:10.1088/2041-8205/802/2/L21.
- M. B. Korsós and R. Erdélyi. On the State of a Solar Active Region Before Flares and CMEs. *Astrophys. J.*, 823:153, June 2016. doi: DOI:10.3847/0004-637X/823/2/153.
- M. B. Korsós, M. K. Georgoulis, N. Gyenge, S. K. Bisoi, S. Yu, S. Poedts, C. J. Nelson, J. Liu, Y. Yan, and R. Erdélyi. Solar Flare Prediction Using Magnetic Field Diagnostics above the Photosphere. *Astrophys. J.*, 896(2):119, June 2020a. doi: 10.3847/1538-4357/ab8fa2.
- I. Kontogiannis, M. K. Georgoulis, S.-H. Park, and J. A. Guerra. Testing and Improving a Set of Morphological Predictors of Flaring Activity. *Solar Phys.*, 293:96, June 2018. doi: DOI:10.1007/s11207-018-1317-2.
- M. K. Georgoulis, V. S. Titov, and Z. Mikić. Non-neutralized Electric Current Patterns in Solar Active Regions: Origin of the Shear-generating Lorentz Force. *Astrophys. J.*, 761:61, December 2012b. doi: DOI:10.1088/0004-637X/761/1/61.
- I. Kontogiannis, M. K. Georgoulis, S.-H. Park, and J. A. Guerra. Non-neutralized Electric Currents in Solar Active Regions and Flare Productivity. *Solar Phys.*, 292:159, November 2017. doi: DOI:10.1007/s11207-017-1185-1.
- Ioannis Kontogiannis, Manolis K. Georgoulis, Jordan A. Guerra, Sung-Hong Park, and D. Shaun Bloomfield. Which Photospheric Characteristics Are Most Relevant to Active-Region Coronal Mass Ejections? *Solar Phys.*, 294(9):130, Sep 2019. doi: DOI:10.1007/s11207-019-1523-6.



- Chloé Guennou, Etienne Pariat, James E Leake, and Nicole Vilmer. Testing predictors of eruptivity using parametric flux emergence simulations. *Journal of Space Weather and Space Climate*, 7:A17, August 2017. doi: DOI:10.1051/swsc/2017015.
- D. A. Falconer, R. L. Moore, and G. A. Gary. Magnetogram Measures of Total Nonpotentiality for Prediction of Solar Coronal Mass Ejections from Active Regions of Any Degree of Magnetic Complexity. *Astrophys. J.*, 689:1433-1442, December 2008b. doi: DOI:10.1086/591045.
- Brian T. Welsch, Yan Li, Peter W. Schuck, and George H. Fisher. What is the Relationship Between Photospheric Flow Fields and Solar Flares? *Astrophys. J.*, 705(1):821-843, November 2009. doi: 10.1088/0004-637X/705/1/821.
- P. W. Schuck. Local Correlation Tracking and the Magnetic Induction Equation. *Astrophys. J. Lett.*, 632(1):L53-L56, October 2005. doi: 10.1086/497633.
- S.-H. Park, J. A. Guerra, P. T. Gallagher, M. K. Georgoulis, and D. S. Bloomfield. Photospheric Shear Flows in Solar Active Regions and Their Relation to Flare Occurrence. *Solar Phys.*, 293:114, August 2018. doi: DOI:10.1007/s11207-018-1336-z.
- P. W. Schuck. Tracking Vector Magnetograms with the Magnetic Induction Equation. *Astrophys. J.*, 683(2):1134-1152, August 2008. doi: 10.1086/589434.
- Brandon Panos and Lucia Kleint. Real-time Flare Prediction Based on Distinctions between Flaring and Non-flaring Active Region Spectra. *Astrophys. J.*, 891(1):17, March 2020. doi: 10.3847/1538-4357/ab700b.
- B. De Pontieu, A. M. Title, J. R. Lemen, G. D. Kushner, D. J. Akin, B. Allard, T. Berger, P. Boerner, M. Cheung, C. Chou, J. F. Drake, D. W. Duncan, S. Freeland, G. F. Heyman, C. Hoffman, N. E. Hurlburt, R. W. Lindgren, D. Mathur, R. Rehse, D. Sabolish, R. Seguin, C. J. Schrijver, T. D. Tarbell, J. P. Wülser, C. J. Wolfson, C. Yanari, J. Mudge, N. Nguyen-Phuc, R. Timmons, R. van Bezooijen, I. Weingrod, R. Brookner, G. Butcher, B. Dougherty, J. Eder, V. Knagenhjelm, S. Larsen, D. Mansir, L. Phan, P. Boyle, P. N. Cheimets, E. E. DeLuca, L. Golub, R. Gates, E. Hertz, S. McKillop, S. Park, T. Perry, W. A. Podgorski, K. Reeves, S. Saar, P. Testa, H. Tian, M. Weber, C. Dunn, S. Eccles, S. A. Jaeggli, C. C. Kankelborg, K. Mashburn, N. Pust, L. Springer, R. Carvalho, L. Kleint, J. Marmie, E. Mazmanian, T. M. D. Pereira, S. Sawyer, J. Strong, S. P. Worden, M. Carlsson, V. H. Hansteen, J. Leenaarts, M. Wiesmann, J. Aloise, K. C. Chu, R. I. Bush, P. H. Scherrer, P. Brekke, J. Martinez-Sykora, B. W. Lites, S. W. McIntosh, H. Uitenbroek, T. J. Okamoto, M. A. Gummie, G. Auken, P. Jerram, P. Pool, and N. Waltham. The Interface Region Imaging Spectrograph (IRIS). *Solar Phys.*, 289(7):2733-2779, July 2014. doi: 10.1007/s11207-014-0485-y.
- C. Gontikakis, I. Kontogiannis, M. K. Georgoulis, C. Guennou, P. Syntelis, S. H. Park, and E. Buchlin. Differential Emission Measure Evolution as a Precursor of Solar Flares. *arXiv e-prints*, art. arXiv:2011.06433, November 2020.
- C. Guennou, F. Auchère, E. Soubrié, K. Bocchialini, S. Parenti, and N. Barbey. On the Accuracy of the Differential Emission Measure Diagnostics of Solar Plasmas. Application to SDO/AIA. I. Isothermal Plasmas. *Astrophys. J. Suppl. Ser.*, 203(2):25, December 2012a. doi: 10.1088/0067-0049/203/2/25.
- C. Guennou, F. Auchère, E. Soubrié, K. Bocchialini, S. Parenti, and N. Barbey. On the Accuracy of the Differential Emission Measure Diagnostics of Solar Plasmas. Application to SDO/AIA. II. Multithermal Plasmas. *Astrophys. J. Suppl. Ser.*, 203(2):26, December 2012b. doi: 10.1088/0067-0049/203/2/26.
- Varad Deshmukh, Thomas E. Berger, Elizabeth Bradley, and James D. Meiss. Leveraging the mathematics of shape for solar magnetic eruption prediction. *Journal of Space Weather and Space Climate*, 10:13, March 2020. doi: 10.1051/swsc/2020014.
- Hu Sun, Ward Manchester, and Yang Chen. Improved and Interpretable Solar Flare Predictions With Spatial and Topological Features of the Polarity Inversion Line Masked Magnetograms. *Space Weather*, 19(12):e02837, December 2021. doi: 10.1029/2021SW002837.

- Jingjing Wang, Yuhang Zhang, Shea A. Hess Webber, Siqing Liu, Xuejie Meng, and Tieyan Wang. Solar Flare Predictive Features Derived from Polarity Inversion Line Masks in Active Regions Using an Unsupervised Machine Learning Algorithm. *Astrophys. J.*, 892(2):140, April 2020. doi: 10.3847/1538-4357/ab7b6c.
- Domenico Cicogna, Francesco Berrilli, Daniele Calchetti, Dario Del Moro, Luca Giovannelli, Federico Benvenuto, Cristina Campi, Sabrina Guastavino, and Michele Piana. Flare-forecasting Algorithms Based on High-gradient Polarity Inversion Lines in Active Regions. *Astrophys. J.*, 915(1):38, July 2021. doi: 10.3847/1538-4357/abfab.
- Breno Raphaldini, Christopher B. Prior, and David MacTaggart. Magnetic Winding as an Indicator of Flare Activity in Solar Active Regions. *Astrophys. J.*, 927(2):156, March 2022. doi: 10.3847/1538-4357/ac4df9.
- Abbas Raboonik, Hossein Safari, Nasibe Alipour, and Michael S. Wheatland. Prediction of Solar Flares Using Unique Signatures of Magnetic Field Images. *Astrophys. J.*, 834(1):11, January 2017. doi: 10.3847/1538-4357/834/1/11.
- Nasibe Alipour, Faranak Mohammadi, and Hossein Safari. Prediction of Flares within 10 Days before They Occur on the Sun. *Astrophys. J. Suppl. Ser.*, 243(2):20, August 2019. doi: 10.3847/1538-4365/ab289b.
- Jingjing Wang, Siqing Liu, Xianzhi Ao, Yuhang Zhang, Tieyan Wang, and Yang Liu. Parameters Derived from the SDO/HMI Vector Magnetic Field Data: Potential to Improve Machine-learning-based Solar Flare Prediction Models. *Astrophys. J.*, 884(2):175, October 2019. doi: 10.3847/1538-4357/ab441b.
- Eric Jonas, Monica Bobra, Vaishaal Shankar, J. Todd Hoeksema, and Benjamin Recht. Flare Prediction Using Photospheric and Coronal Image Data. *Solar Phys.*, 293(3):48, March 2018. doi: 10.1007/s11207-018-1258-9.
- Naoto Nishizuka, Yûki Kubo, Komei Sugiura, Mitsue Den, and Mamoru Ishii. Operational solar flare prediction model using Deep Flare Net. *Earth, Planets and Space*, 73(1):64, December 2021. doi: 10.1186/s40623-021-01381-9.
- Ali K. Abed, Rami Qahwaji, and Ahmed Abed. The automated prediction of solar flares from SDO images using deep learning. *Advances in Space Research*, 67(8):2544–2557, April 2021. doi: 10.1016/j.asr.2021.01.042.
- H. Carmichael. A Process for Flares. In *NASA Special Publication*, volume 50, page 451. 1964.
- P. A. Sturrock. Model of the High-Energy Phase of Solar Flares. *Nature*, 211(5050):695–697, August 1966. doi: 10.1038/211695a0.
- T. Hirayama. Theoretical Model of Flares and Prominences. I: Evaporating Flare Model. *Solar Phys.*, 34(2):323–338, February 1974. doi: 10.1007/BF00153671.
- R. A. Kopp and G. W. Pneuman. Magnetic reconnection in the corona and the loop prominence phenomenon. *Solar Phys.*, 50(1):85–98, October 1976. doi: 10.1007/BF00206193.
- V. S. Titov and P. Démoulin. Basic topology of twisted magnetic configurations in solar flares. *Astron. Astrophys.*, 351:707–720, November 1999.
- A. A. van Ballegoijen and P. C. H. Martens. Formation and Eruption of Solar Prominences. *Astrophys. J.*, 343:971, August 1989. doi: 10.1086/167766.
- G. Aulanier, M. Janvier, and B. Schmieder. The standard flare model in three dimensions. I. Strong-to-weak shear transition in post-flare loops. *Astron. Astrophys.*, 543:A110, July 2012. doi: 10.1051/0004-6361/201219311.
- G. Aulanier, P. Démoulin, C. J. Schrijver, M. Janvier, E. Pariat, and B. Schmieder. The standard flare model in three dimensions. II. Upper limit on solar flare energy. *Astron. Astrophys.*, 549:A66, January 2013. doi: 10.1051/0004-6361/201220406.

- M. Janvier, G. Aulanier, E. Pariat, and P. Démoulin. The standard flare model in three dimensions. III. Slip-running reconnection properties. *Astron. Astrophys.*, 555:A77, July 2013. doi: 10.1051/0004-6361/201321164.
- M. A. Berger and G. B. Field. The topological properties of magnetic helicity. *Journal of Fluid Mechanics*, 147:133–148, October 1984. doi: 10.1017/S0022112084002019.
- Kostas Tziotziou, Manolis K. Georgoulis, and Nour-Eddine Raouafi. The Magnetic Energy-Helicity Diagram of Solar Active Regions. *Astrophys. J. Lett.*, 759(1):L4, November 2012. doi: 10.1088/2041-8205/759/1/L4.
- Kostas Tziotziou, Manolis K. Georgoulis, and Yang Liu. Interpreting Eruptive Behavior in NOAA AR 11158 via the Region’s Magnetic Energy and Relative-helicity Budgets. *Astrophys. J.*, 772(2):115, August 2013. doi: 10.1088/0004-637X/772/2/115.
- Manolis K. Georgoulis, Alexander Nindos, and Hongqi Zhang. The source and engine of coronal mass ejections. *Philosophical Transactions of the Royal Society of London Series A*, 377(2148):20180094, July 2019. doi: DOI:10.1098/rsta.2018.0094.
- Sung-hong Park, Jongchul Chae, and Haimin Wang. Productivity of Solar Flares and Magnetic Helicity Injection in Active Regions. *Astrophys. J.*, 718(1):43–51, July 2010. doi: 10.1088/0004-637X/718/1/43.
- S.-H. Park, K.-S. Cho, S.-C. Bong, P. Kumar, J. Chae, R. Liu, and H. Wang. The Occurrence and Speed of CMEs Related to Two Characteristic Evolution Patterns of Helicity Injection in Their Solar Source Regions. *Astrophys. J.*, 750:48, May 2012. doi: DOI:10.1088/0004-637X/750/1/48.
- T. Török and B. Kliem. Confined and Ejective Eruptions of Kink-unstable Flux Ropes. *Astrophys. J. Lett.*, 630(1):L97–L100, September 2005. doi: 10.1086/462412.
- Y. Liu. Magnetic Field Overlying Solar Eruption Regions and Kink and Torus Instabilities. *Astrophys. J. Lett.*, 679(2):L151, June 2008. doi: 10.1086/589282.
- F. P. Zuccarello, D. B. Seaton, M. Mierla, S. Poedts, L. A. Rachmeler, P. Romano, and F. Zuccarello. Observational Evidence of Torus Instability as Trigger Mechanism for Coronal Mass Ejections: The 2011 August 4 Filament Eruption. *Astrophys. J.*, 785(2):88, April 2014. doi: 10.1088/0004-637X/785/2/88.
- F. P. Zuccarello, G. Aulanier, and S. A. Gilchrist. Critical Decay Index at the Onset of Solar Eruptions. *Astrophys. J.*, 814:126, December 2015. doi: DOI:10.1088/0004-637X/814/2/126.
- N. Vasantharaju, P. Vemareddy, B. Ravindra, and V. H. Doddamani. Statistical Study of Magnetic Nonpotential Measures in Confined and Eruptive Flares. *Astrophys. J.*, 860(1):58, June 2018. doi: 10.3847/1538-4357/aac272.
- Sanchita Pal, Dibyendu Nandy, Nandita Srivastava, Nat Gopalswamy, and Suman Panda. Dependence of Coronal Mass Ejection Properties on Their Solar Source Active Region Characteristics and Associated Flare Reconnection Flux. *Astrophys. J.*, 865(1):4, September 2018. doi: 10.3847/1538-4357/aada10.
- Paolo Pagano, Duncan H. Mackay, and Stephanie L. Yardley. A Prospective New Diagnostic Technique for Distinguishing Eruptive and Noneruptive Active Regions. *Astrophys. J.*, 883(2):112, October 2019a. doi: 10.3847/1538-4357/ab3e42.
- Paolo Pagano, Duncan H. Mackay, and Stephanie L. Yardley. A New Space Weather Tool for Identifying Eruptive Active Regions. *Astrophys. J.*, 886(2):81, December 2019b. doi: 10.3847/1538-4357/ab4cfl.
- Pei Hsuan Lin, Kanya Kusano, Daikou Shiota, Satoshi Inoue, K. D. Leka, and Yuta Mizuno. A New Parameter of the Photospheric Magnetic Field to Distinguish Eruptive-flare Producing Solar Active Regions. *Astrophys. J.*, 894(1):20, May 2020. doi: 10.3847/1538-4357/ab822c.

- Ting Li, Xudong Sun, Yijun Hou, Anqin Chen, Shuhong Yang, and Jun Zhang. A New Magnetic Parameter of Active Regions Distinguishing Large Eruptive and Confined Solar Flares. *Astrophys. J. Lett.*, 926(2):L14, February 2022. doi: 10.3847/2041-8213/ac5251.
- K. Kusano, T. Maeshiro, T. Yokoyama, and T. Sakurai. Measurement of Magnetic Helicity Injection and Free Energy Loading into the Solar Corona. *Astrophys. J.*, 577(1):501–512, September 2002. doi: 10.1086/342171.
- B. J. LaBonte, M. K. Georgoulis, and D. M. Rust. Survey of Magnetic Helicity Injection in Regions Producing X-Class Flares. *Astrophys. J.*, 671(1):955–963, December 2007. doi: 10.1086/522682.
- Sung-Hong Park, Jeongwoo Lee, G. S. Choe, Jongchul Chae, Hyewon Jeong, Guo Yang, Ju Jing, and Haimin Wang. The Variation of Relative Magnetic Helicity around Major Flares. *Astrophys. J.*, 686(2):1397–1403, October 2008. doi: 10.1086/591117.
- M. K. Georgoulis. Toward an Efficient Prediction of Solar Flares: Which Parameters, and How? *Entropy*, 15(11):5022–5052, November 2013. doi: 10.3390/e15115022.
- M. B. Korsós, P. Romano, H. Morgan, Y. Ye, R. Erdélyi, and F. Zuccarello. Differences in Periodic Magnetic Helicity Injection Behavior between Flaring and Non-flaring Active Regions: Case Study. *Astrophys. J. Lett.*, 897(2):L23, July 2020b. doi: 10.3847/2041-8213/ab9d7a.
- Sz. Soós, M. B. Korsós, H. Morgan, and R. Erdélyi. On the Differences in the Periodic Behavior of Magnetic Helicity Flux in Flaring Active Regions with and without X-class Events. *Astrophys. J.*, 925(2):129, February 2022. doi: 10.3847/1538-4357/ac4094.
- M. S. Wheatland. A statistical solar flare forecast method. *Space Weather*, 3(7):S07003, July 2005. doi: 10.1029/2004SW000131.
- David A. Falconer, Ronald L. Moore, Abdulnasser F. Barghouty, and Igor Khazanov. MAG4 versus alternative techniques for forecasting active region flare productivity. *Space Weather*, 12(5):306–317, May 2014. doi: 10.1002/2013SW001024.
- Hao Liu, Chang Liu, Jason T. L. Wang, and Haimin Wang. Predicting Solar Flares Using a Long Short-term Memory Network. *Astrophys. J.*, 877(2):121, June 2019. doi: 10.3847/1538-4357/ab1b3c.
- Xin Huang, Daren Yu, Qinghua Hu, Huaning Wang, and Yanmei Cui. Short-Term Solar Flare Prediction Using Predictor Teams. *Solar Phys.*, 263(1-2):175–184, May 2010. doi: 10.1007/s11207-010-9542-3.
- Daren Yu, Xin Huang, Qinghua Hu, Rui Zhou, Huaning Wang, and Yanmei Cui. Short-term Solar Flare Prediction Using Multiresolution Predictors. *Astrophys. J.*, 709(1):321–326, January 2010a. doi: 10.1088/0004-637X/709/1/321.
- Daren Yu, Xin Huang, Huaning Wang, Yanmei Cui, Qinghua Hu, and Rui Zhou. Short-term Solar Flare Level Prediction Using a Bayesian Network Approach. *Astrophys. J.*, 710(1):869–877, February 2010b. doi: 10.1088/0004-637X/710/1/869.
- Yang Chen, Ward B. Manchester, Alfred O. Hero, Gabor Toth, Benoit DuFumier, Tian Zhou, Xiantong Wang, Haonan Zhu, Zeyu Sun, and Tamas I. Gombosi. Identifying Solar Flare Precursors Using Time Series of SDO/HMI Images and SHARP Parameters. *Space Weather*, 17(10):1404–1426, October 2019. doi: 10.1029/2019SW002214.
- Hao Liu, Chang Liu, Jason T. L. Wang, and Haimin Wang. Predicting Coronal Mass Ejections Using SDO/HMI Vector Magnetic Data Products and Recurrent Neural Networks. *Astrophys. J.*, 890(1):12, February 2020. doi: 10.3847/1538-4357/ab6850.
- Kangjin Lee, Y. J. Moon, Jin-Yi Lee, Kyoung-Sun Lee, and Hyeonock Na. Solar Flare Occurrence Rate and Probability in Terms of the Sunspot Classification Supplemented with Sunspot Area and Its Changes. *Solar Phys.*, 281(2):639–650, December 2012. doi: 10.1007/s11207-012-0091-9.

- Aoife E. McCloskey, Peter T. Gallagher, and D. Shaun Bloomfield. Flare forecasting using the evolution of McIntosh sunspot classifications. *Journal of Space Weather and Space Climate*, 8:A34, June 2018. doi: 10.1051/swsc/2018022.
- A. Al-Ghraibah, L. E. Boucheron, and R. T. J. McAteer. An automated classification approach to ranking photospheric proxies of magnetic energy build-up. *Astron. Astrophys.*, 579:A64, July 2015. doi: 10.1051/0004-6361/201525978.
- Laura E. Boucheron, Amani Al-Ghraibah, and R. T. James McAteer. Prediction of Solar Flare Size and Time-to-Flare Using Support Vector Machine Regression. *Astrophys. J.*, 812(1):51, October 2015. doi: 10.1088/0004-637X/812/1/51.
- N. Nishizuka, K. Sugiura, Y. Kubo, M. Den, S. Watari, and M. Ishii. Solar Flare Prediction Model with Three Machine-learning Algorithms using Ultraviolet Brightening and Vector Magnetograms. *Astrophys. J.*, 835(2):156, February 2017. doi: 10.3847/1538-4357/835/2/156.
- K. D. Leka, Graham Barnes, and Eric Wagner. The NWRA Classification Infrastructure: description and extension to the Discriminant Analysis Flare Forecasting System (DAFFS). *Journal of Space Weather and Space Climate*, 8:A25, April 2018. doi: 10.1051/swsc/2018004.
- Eo-Jin Lee, Sung-Hong Park, and Yong-Jae Moon. Flare Productivity of Major Flaring Solar Active Regions: A Time-Series Study of Photospheric Magnetic Properties. *Solar Phys.*, 293(12):159, December 2018. doi: 10.1007/s11207-018-1381-7.
- Eo-Jin Lee, Sung-Hong Park, and Yong-Jae Moon. Time Series Analysis of Photospheric Magnetic Parameters of Flare-Quiet Versus Flaring Active Regions: Scaling Properties of Fluctuations. *Solar Phys.*, 295(9):123, September 2020. doi: 10.1007/s11207-020-01690-4.
- Lucas A. Pauker, Monica G. Bobra, and Eric Jonas. Predicting Solar Flares Using Time Series Analysis. *Research Notes of the American Astronomical Society*, 3(10):157, October 2019. doi: 10.3847/2515-5172/ab4db0.
- Rafal A. Angryk, Petrus C. Martens, Berkay Aydin, Dustin Kempton, Sushant S. Mahajan, Sunitha Basodi, Azim Ahmadzadeh, Xumin Cai, Soukaina Filali Boubrahimi, Shah Muhammad Hamdi, Michael A. Schuh, and Manolis K. Georgoulis. Multivariate time series dataset for space weather data analytics. *Nature Scientific Data*, 7(1):227, July 2020. doi: 10.1038/s41597-020-0548-x.
- Angelos Vourlidas. Mission to the Sun-Earth L<sub>5</sub> Lagrangian Point: An Optimal Platform for Space Weather Research. *Space Weather*, 13(4):197–201, April 2015. doi: 10.1002/2015SW001173.
- Carolus J. Schrijver, Kirsti Kauristie, Alan D. Aylward, Clezio M. Denardini, Sarah E. Gibson, Alexi Glover, Nat Gopalswamy, Manuel Grande, Mike Hapgood, Daniel Heynderickx, Norbert Jakowski, Vladimir V. Kalegaev, Giovanni Lapenta, Jon A. Linker, Siqing Liu, Cristina H. Mandrini, Ian R. Mann, Tsutomu Nagatsuma, Dibyendu Nandy, Takahiro Obara, T. Paul O’Brien, Terrance Onsager, Hermann J. Opgenoorth, Michael Terkildsen, Cesar E. Valladares, and Nicole Vilmer. Understanding space weather to shield society: A global road map for 2015-2025 commissioned by COSPAR and ILWS. *Advances in Space Research*, 55(12):2745–2807, June 2015. doi: DOI:10.1016/j.asr.2015.03.023.
- G. Barnes, K. D. Leka, C. J. Schrijver, T. Colak, R. Qahwaji, O. W. Ashamari, Y. Yuan, J. Zhang, R. T. J. McAteer, D. S. Bloomfield, P. A. Higgins, P. T. Gallagher, D. A. Falconer, M. K. Georgoulis, M. S. Wheatland, C. Balch, T. Dunn, and E. L. Wagner. A Comparison of Flare Forecasting Methods. I. Results from the ‘All-Clear’ Workshop. *Astrophys. J.*, 829:89, October 2016. doi: DOI:10.3847/0004-637X/829/2/89.
- Cristina Campi, Federico Benvenuto, Anna Maria Massone, D. Shaun Bloomfield, Manolis K. Georgoulis, and Michele Piana. Feature Ranking of Active Region Source Properties in Solar Flare Forecasting and the Uncompromised Stochasticity of Flare Occurrence. *Astrophys. J.*, 883(2):150, October 2019. doi: 10.3847/1538-4357/ab3c26.

- Philip Judge, Matthias Rempel, Rana Ezzeddine, Lucia Kleint, Ricky Egeland, Svetlana V. Berdyugina, Thomas Berger, Paul Bryans, Joan Burkepile, Rebecca Centeno, Giuliana de Toma, Mausumi Dikpati, Yuhong Fan, Holly Gilbert, and Daniela A. Lacatus. Measuring the Magnetic Origins of Solar Flares, Coronal Mass Ejections, and Space Weather. *Astrophys. J.*, 917(1):27, August 2021. doi: 10.3847/1538-4357/ac081f.
- Tahar Amari, Aurélien Canou, Jean-Jacques Aly, Francois Delyon, and Frédéric Alauzet. Magnetic cage and rope as the key for solar eruptions. *Nature*, 554(7691):211–215, February 2018. doi: 10.1038/nature24671.
- A. Bagnall, J. Lines, A. Bostrom, J. Large, and E. Keogh. The great time series classification bake off: a review and experimental evaluation of recent algorithmic advances. *Data Min Knowl Disc*, 31:606, May 2017. doi: 10.1007/s10618-016-0483-9.
- D. Müller, O. C. St. Cyr, I. Zouganelis, H. R. Gilbert, R. Marsden, T. Nieves-Chinchilla, E. Antonucci, F. Auchère, D. Berghmans, T. S. Horbury, R. A. Howard, S. Krucker, M. Maksimovic, C. J. Owen, P. Rochus, J. Rodriguez-Pacheco, M. Romoli, S. K. Solanki, R. Bruno, M. Carlsson, A. Fludra, L. Harra, D. M. Hassler, S. Livi, P. Louarn, H. Peter, U. Schühle, L. Teriaca, J. C. del Toro Iniesta, R. F. Wimmer-Schweingruber, E. Marsch, M. Velli, A. De Groof, A. Walsh, and D. Williams. The Solar Orbiter mission. Science overview. *Astron. Astrophys.*, 642:A1, October 2020. doi: 10.1051/0004-6361/202038467.
- Thomas R. Rimmele, Mark Warner, Stephen L. Keil, Philip R. Goode, Michael Knölker, Jeffrey R. Kuhn, Robert R. Rosner, Joseph P. McMullin, Roberto Casini, Haosheng Lin, Friedrich Wöger, Oskar von der Lühe, Alexandra Tritschler, Alisdair Davey, Alfred de Wijn, David F. Elmore, André Fehlmann, David M. Harrington, Sarah A. Jaeggli, Mark P. Rast, Thomas A. Schad, Wolfgang Schmidt, Mihalis Mathioudakis, Donald L. Mickey, Tetsu Anan, Christian Beck, Heather K. Marshall, Paul F. Jeffers, Jacobus M. Oschmann, Andrew Beard, David C. Berst, Bruce A. Cowan, Simon C. Craig, Eric Cross, Bryan K. Cummings, Colleen Donnelly, Jean-Benoit de Vanssay, Arthur D. Eigenbrot, Andrew Ferayorni, Christopher Foster, Chriselle Ann Galapon, Christopher Gedrites, Kerry Gonzales, Bret D. Goodrich, Brian S. Gregory, Stephanie S. Guzman, Stephen Guzzo, Steve Hegwer, Robert P. Hubbard, John R. Hubbard, Erik M. Johansson, Luke C. Johnson, Chen Liang, Mary Liang, Isaac McQuillen, Christopher Mayer, Karl Newman, Brialyn Onodera, LeEllen Phelps, Myles M. Puentes, Christopher Richards, Lukas M. Rimmele, Predrag Sekulic, Stephan R. Shimko, Brett E. Simison, Brett Smith, Erik Starman, Stacey R. Sueoka, Richard T. Summers, Aimee Szabo, Louis Szabo, Stephen B. Wampler, Timothy R. Williams, and Charles White. The Daniel K. Inouye Solar Telescope - Observatory Overview. *Solar Phys.*, 295(12):172, December 2020. doi: 10.1007/s11207-020-01736-7.
- C. Quintero Noda, R. Schlichenmaier, L. R. Bellot Rubio, M. G. Löfdahl, E. Khomenko, J. Jurcak, J. Leenaarts, C. Kuckein, S. J. González Manrique, S. Gunar, C. J. Nelson, J. de la Cruz Rodríguez, K. Tziotziou, G. Tsiropoula, G. Aulanier, M. Collados, and the EST team. The European Solar Telescope. *arXiv e-prints*, art. arXiv:2207.10905, July 2022.
- Louise K. Harra, Sarah Matthews, J. L. Culhane, Mark C. M. Cheung, Eduard P. Kontar, and Hirohisa Hara. The Location of Non-thermal Velocity in the Early Phases of Large Flares—Revealing Pre-eruption Flux Ropes. *Astrophys. J.*, 774(2):122, September 2013. doi: 10.1088/0004-637X/774/2/122.
- P. Syntelis, C. Gontikakis, S. Patsourakos, and K. Tsinganos. The spectroscopic imprint of the pre-eruptive configuration resulting into two major coronal mass ejections. *Astron. Astrophys.*, 588: A16, April 2016. doi: 10.1051/0004-6361/201526829.